

**ULTRASOUND TO CT REGISTRATION OF THE LUMBAR
SPINE: A CLINICAL FEASIBILITY STUDY**

by

SIMRIN NAGPAL

A thesis submitted to the
School of Computing
in conformity with the requirements for
the degree of Master of Science

Queen's University
Kingston, Ontario, Canada
August 2013

Copyright © Simrin Nagpal, 2013

Abstract

Spine needle injections are widely applied to alleviate pain and to remove nerve sensation through anesthesia. Current treatment is performed either blindly having no image guidance or using fluoroscopy or computed tomography (CT). Both CT and fluoroscopy guidance expose patients to ionizing radiation. Alternatively, ultrasound (US) guidance for spine needle procedures is becoming more prevalent since US is a non-ionizing and more accessible image modality. An inherent challenge to US imaging of the spine is the acoustic shadows created by the bony structures of the vertebra limiting visibility.

It is challenging to use US as the sole imaging modality for intraoperative guidance of spine needle injections. However, it is possible to enhance the anatomical information through a preoperative diagnostic CT. To achieve this, image registration between the CT and the US images is proposed in this thesis. Image registration integrates the anatomical information from the CT with the US images. The aligned CT augments anatomical visualization for the clinician during spinal interventions.

To align the preoperative CT and intraoperative US, a novel registration pipeline is presented that involves automatic global and multi-vertebrae registration. The registration pipeline is composed of two distinct phases: preoperative and intraoperative. Preoperatively, points are selected between adjacent vertebrae that act as

artificial springs. Intraoperatively, the lumbar spine is first aligned between the CT and US followed by a multi-vertebrae registration. The artificial springs are used to constrain the movement of the individually transformed vertebrae to ensure the optimal alignment is a pose of the lumbar spine that is physically possible.

Validation of the algorithm is performed on five clinical patient datasets. A protocol for US data collection was created to eliminate variability in the quality of acquired US images. The registration pipeline was able to register the datasets from initial misalignments of up to 25 mm with a mean TRE of 1.17 mm. From these results, it is evident that the proposed registration pipeline offers a robust registration between clinical CT and US data.

Statement of Co-Authorship

The work presented in this thesis was accomplished under the supervision of Dr. Parvin Mousavi and Dr. Purang Abolmaesumi, and the guidance of Dr. Tamas Ungi and Dr. Ilker Hacihaliloglu who also provided feedback and corrections to the manuscript. Dr. Tamas Ungi and Dr. Dan Borschneck selected landmark points that were used to validate the registration. Dr. Ilker Hacihaliloglu provided the local phase filtering for the CT and US datasets. Abtin Rasoulian automatically segmented the vertebrae in the CT images and helped with the incorporation of springs in the multi-vertebrae registration. Simrin Nagpal, Abtin Rasoulian, Saman Nouranian and Samira Sojoudi jointly acquired the clinical data and developed the US data collection protocol. Otherwise, the material presented in this thesis is the original work of the author.

Preliminary plans to refine this thesis into a future journal article submission with the previously mentioned co-authors have been established.

Acknowledgments

I would first like to thank my supervisors Dr. Parvin Mousavi and Dr. Purang Abolmaesumi for their guidance throughout my thesis project. Dr. Tamas Ungi, Dr. Ilker Hacihaliloglu and Abtin Rasoulian, thank you for your advice, guidance and interest in this thesis. Thank you Dr. Dan Borschneck for the clinical insight and discussion. I would also like to thank Dr. Gabor Fichtinger and Dr. Andras Lasso for providing opportunities for growth.

Thanks to the members of the Med-i and PERK labs for your support. Special thanks to Melissa for your true friendship. This journey would not have been the same without you. Saman and Samira, thank you for welcoming me at UBC.

To my friends, thanks for all of the laughter and memories that made my Queen's experience so enjoyable. Anna and Laura, you have been through all of this with me since the booga-bouga days.

Finally, I would not be where I am today without the unconditional love and support from my parents Daljit and Kamal, and my sister Sonya.

I dedicate this thesis to Trisha as her example guided me to always strive for excellence.

“...let us step out into the night and pursue that flighty temptress, adventure.” - Albus Dumbledore

Glossary

1D 1 Dimension/Dimensional.

2D 2 Dimensions/Dimensional.

3D 3 Dimensions/Dimensional.

CPD Coherent Point Drift.

CT Computed Tomography.

EM Electromagnetic.

GMM Gaussian Mixture Model.

GPS Guidance Positioning System.

Intraoperative during the intervention.

MI Mutual Information.

PDF Probability Density Function.

PLUS Public software Library for UltraSound imaging research.

Preoperative prior to the intervention.

SSM Statistical Shape Model.

TRE Target Registration Error.

UKF Unscented Kalman Filter.

US Ultrasound.

Contents

Abstract	i
Statement of Co-Authorship	iii
Acknowledgments	iv
Glossary	v
Contents	vii
List of Figures	ix
List of Tables	xv
Chapter 1: Introduction	1
1.1 Motivation	1
1.2 Thesis Objectives	3
1.3 Thesis Contributions	5
1.4 Thesis Outline	5
Chapter 2: Background	7
2.1 Percutaneous Lumbar Spine Interventions	7
2.1.1 Lumbar Spine Anatomy	8
2.1.2 Spinal Injections	12
2.2 Ultrasound-guided Interventions of the Spine	14
2.3 Medical Image Registration	16
2.3.1 CT to US Registration of the Spine	18
2.4 Medical Imaging Software	27
2.4.1 Matlab	27
2.4.2 PLUS	28
2.4.3 Slicer	29
2.5 Summary	30

Chapter 3: Experimental Design	31
3.1 CT Data Acquisition	31
3.2 Tracked US Data Acquisition	32
3.2.1 Hardware Setup	33
3.2.2 Software Setup	33
3.2.3 Patient Setup	34
3.2.4 US scanning	36
3.3 Validating the Alignment of the US and CT Images	39
3.4 Summary	41
Chapter 4: Methods	43
4.1 Global Intensity-based Registration	46
4.1.1 Phase-based CT Bone Surface Segmentation	48
4.1.2 Phase-based US Bone Surface Segmentation	51
4.1.3 Rigid Phase CT to US Registration	53
4.2 Global Point-based Registration	54
4.2.1 Single Pixel US Bone Surface Segmentation	55
4.2.2 Point-based Global Rigid Registration	56
4.2.3 Multi-vertebrae Point-based Registration	60
4.3 Summary	65
Chapter 5: Results and Discussion	66
5.1 CT to US Registration Results using the Proposed Pipeline	68
5.1.1 The Effect of the Intensity-based Registration Step	76
5.1.2 The Effect of using the Unmodified Single Pixel US Bone Surface	78
5.1.3 The Effect of the Global Point-based Registration Step	80
5.1.4 The Effect of Springs in the Piecewise Point-based Registration Step	83
5.2 Summary	86
Chapter 6: Conclusions and Future Work	88
6.1 Summary of Conclusions	88
6.2 Future Work	90
Bibliography	92

List of Figures

1.1	US guidance system where preoperative CT is aligned with intraoperative US.	4
2.1	The human standardized anatomical position along with the three reference planes and six anatomical directions. This figure is modified from [48].	8
2.2	Sagittal CT slice demonstrating the five vertebrae that make up the lumbar spine.	9
2.3	3D rendering of the L4 and L5 vertebrae from the CT. Annotations in yellow describe various relevant spine anatomy.	10
2.4	Sagittal US slice of the lumbar spine with anatomical annotations in red. The letters I, S, A, P refer to the anatomical directions inferior, superior, anterior and posterior, respectively.	10
2.5	3D rendering of the L4 and L5 vertebrae from the CT to show the location of the epidural space in blue relative to the spinal cord and dura.	11
2.6	3D rendering of the L4 and L5 vertebrae from the CT intersecting with a sagittal US plane. The letters I, S, A, P refer to the anatomical directions inferior, superior, anterior and posterior, respectively.	11

2.7	3D rendering of the L4 and L5 vertebrae from the CT demonstrating an injection into the epidural space.	13
2.8	3D rendering of the L4 and L5 vertebrae from the CT demonstrating an injection into the facet joint.	14
3.1	Data acquisition system for tracked US. SonixTouch (Ultrasonix, Richmond, BC) ultrasound scanner; GPS extension (Ascension DriveBay electromagnetic tracker); tracked C5-2 curvilinear transducer (Ultrasonix); 3D position sensors affixed to the transducer and patient. This figure is modified from [56].	34
3.2	Volunteer demonstrating the subject's position during the US data acquisition. The subject is in the prone position with a pillow under their stomach.	35
3.3	Reference sensor holder that orients the reference sensor according to the anatomical directions.	36
3.4	Scan styles for US data acquisition with example US images. Annotations of anatomy are shown in red.(a) transverse U-shaped scan; (b) transverse midline scan; (c) sagittal zigzag scan.	38
3.5	One case of quantitative validation of the CT to US alignment using lamina landmarks placed on the US. Original positions of landmarks are shown in yellow after the alignment of the CT to the US and the transformed positions are shown in blue. (a) CT aligned to original position of US lamina landmarks; (b) CT and lamina landmarks transformed by initial perturbation; (c) CT and lamina landmarks transformed by CT to US transformation found through registration pipeline.	40

3.6	One case of qualitative validation of the CT to US alignment using posterior dura landmarks on the US signifying where a needle's target would be for spinal anesthesia. Landmarks are shown in yellow.	41
4.1	General overview of the CT to US registration workflow.	46
4.2	Expansion of Figure 4.1 to show details of the preprocessing for the intensity-based rigid registration.	48
4.3	Sagittal CT slice overlaid in yellow with the phase filtered and raycasted bone surface. (a) CT slice from patient 3 with its corresponding raycasted bone surface. (b) CT slice from patient 5 with its corresponding raycasted bone surface.	50
4.4	Sagittal CT slice overlaid with the inverse Euclidean distance map of the enhanced bone surface. (a) Inverse distance map corresponding to the bone surface in Figure 4.3(a). (b) Inverse distance map corresponding to the bone surface in Figure 4.3(b).	50
4.5	Sagittal US slice. The phase filtered and raycasted bone surface is overlaid on the US slice and is shown in yellow. (a) US slice from patient 3. (b) US slice from patient 5.	53
4.6	Sagittal US slice overlaid in yellow with the single pixel bone surface. (a) US slice using the modified algorithm; (b) US slice using the original algorithm.	56
4.7	General overview of the point-based global rigid CPD registration. This figure is expanded from Figure 4.1.	57
4.8	General overview of the multi-vertebrae point-based registration. This figure is expanded from Figure 4.1.	61

4.9 Sagittal slice of a CT demonstrating three spring points that were manually chosen between two adjacent vertebra. Two are approximately at the midpoint in the space between two adjacent vertebral bodies (shown in red). One point is within the facet joint (shown in green).	63
5.1 Plot of the final mean TRE (mm) for all vertebrae between the CT and US data after the registration pipeline given the initial TRE (mm) after the random initial misalignment. (a) patient 1; (b) patient 2; (c) patient 3; (d) patient 4; (e) patient 5.	69
5.2 3D rendering of CT vertebrae with points on the posterior dura between two vertebrae (represented in yellow) on the top right and sagittal (bottom left), transverse (top left) and coronal (bottom right) planes showing US slices with the CT contours overlaid for patient 1.	71
5.3 3D rendering of CT vertebrae with points on the posterior dura between two vertebrae (represented in yellow) on the top right and sagittal (bottom left), transverse (top left) and coronal (bottom right) planes showing US slices with the CT contours overlaid for patient 2.	72
5.4 3D rendering of CT vertebrae with points on the posterior dura between two vertebrae (represented in yellow) on the top right and sagittal (bottom left), transverse (top left) and coronal (bottom right) planes showing US slices with the CT contours overlaid for patient 3.	73

5.5	3D rendering of CT vertebrae with points on the posterior dura between two vertebrae (represented in yellow) on the top right and sagittal (bottom left), transverse (top left) and coronal (bottom right) planes showing US slices with the CT contours overlaid for patient 4.	74
5.6	3D rendering of CT vertebrae with points on the posterior dura between two vertebrae (represented in yellow) on the top right and sagittal (bottom left), transverse (top left) and coronal (bottom right) planes showing US slices with the CT contours overlaid for patient 5.	75
5.7	Plot of the final TRE (mm) between the CT and US data after the modified registration pipeline given the initial TRE (mm) following the random initial misalignment. The pipeline was modified to eliminate the intensity-based registration step. (a) patient 1; (b) patient 2;(c) patient 3; (d) patient 4; (e) patient 5.	77
5.8	Plot of the final TRE (mm) between the CT and US data after the modified registration pipeline versus initial TRE (mm) following the random initial misalignment. The pipeline was modified to use the unmodified single pixel US bone surface.(a) patient 1; (b) patient 2;(c) patient 3; (d) patient 4; (e) patient 5.	79

5.9	Plot of the final TRE (mm) between the CT and US data after the modified registration pipeline given the initial TRE (mm) following the random initial misalignment. The pipeline was modified to eliminate the global point-based registration step. (a) patient 1; (b) patient 2;(c) patient 3; (d) patient 4; (e) patient 5.	82
5.10	Plot of the final TRE (mm) between the CT and US data after the modified registration pipeline given the initial TRE (mm) following the random initial misalignment. The pipeline was modified to remove the springs in the piecewise point-based registration. (a) patient 1; (b) patient 2;(c) patient 3; (d) patient 4; (e) patient 5.	85
5.11	Registration result after one run for patient 2 showing that the lumbar spine pose is not physically possible.	86

List of Tables

3.1	Demographics of subjects recruited for US imaging.	32
5.1	Lumbar vertebrae in the CT that are registered for each of the five patients.	67
5.2	Runtime range in seconds for each of the registration components in the pipeline.	68
5.3	Mean TRE (mm), maximum point distance (mm) and total success rate from the CT to US registration for the five patients using the full registration pipeline.	70
5.4	Mean TRE (mm) and maximum point distance (mm) from the CT to US registration for the five patients using a modified registration pipeline, where the intensity-based registration step is not performed.	78
5.5	Mean TRE (mm) and maximum point distance (mm) from the CT to US registration for the five patients using a modified registration pipeline, where the unmodified single pixel US bone surface was used.	80
5.6	Mean TRE (mm) and maximum point distance (mm) from the CT to US registration for the 5 patients using a modified registration pipeline, where the global point-based registration step is not performed.	83

5.7 Mean TRE (mm) and maximum point distance (mm) from the CT to US registration for the five patients using a modified registration pipeline, where the springs in the piecewise point-based registration are not used.	86
---	----

Chapter 1

Introduction

1.1 Motivation

Spine needle injections are commonly used for analgesia to relieve pain and anesthesia to remove nerve sensation. Injections into the target region in the spine are particularly challenging due to the deep targets that may not be identified through palpation [55]. For instance, it was previously shown that inaccurate identification of the spaces between the lumbar vertebrae was seen in 40 to 59% of subjects when only palpation was used [5].

An example of a common clinical procedure to treat chronic lower back pain is an injection into the facet joint. Between 25 to 45% of chronic lower back is attributed to the facet joint [15]. Injections into this region are particularly challenging due to the deep location, proximity to nerve tissue and the narrow joint space. These challenges make it difficult to provide accurate treatment to the target area when the procedure is performed without guidance. The current gold standard to guide the injection is fluoroscopy or computed tomography (CT). However, there are several drawbacks to these image modalities, including ionizing radiation to the patient and physician.

Epidural injections represent another common percutaneous injection into the spine. They are used in surgery as an alternative to general anesthesia as well as in obstetrics during delivery. Fluoroscopy may only be used in non-obstetric cases because it emits radiation. Blind palpation can be used as a non-ionizing alternative in obstetrics. However, this can be challenging in obese patients or those with a diseased spine [1]. In these cases, an alternative guidance modality is needed for this procedure.

Intraoperative ultrasound (US) guidance for spine needle procedures is becoming more popular, since US is a non-ionizing and more accessible image modality compared to fluoroscopy or CT [12]. US has not become the standard of care for spine needle injections due to the difficulty associated with its interpretation of anatomy. Specifically, acoustic shadows from the bony structures of vertebrae limit the visibility of anatomical targets, such as facet joints in US images.

To enhance the quality of US images, three dimensional (3D) anatomical information (e.g. from a preoperative CT) can be integrated with the intraoperative US images through image registration. Image registration transforms the anatomical information (e.g. preoperative CT images) into the same coordinate system as the intraoperative US images. Using US guidance eliminates radiation associated with intraoperative CT or fluoroscopy and facilitates the interpretation of US images during spinal interventions.

1.2 Thesis Objectives

The research described in this thesis is a component of a large-scale project involving the development of a real-time US-guided system for percutaneous needle interventions for the spine. In this system, the US images are registered to a preoperative diagnostic CT to augment anatomical information without further radiation. To eliminate radiation completely in cases where a diagnostic CT is unavailable, a statistical shape model (SSM) of the lumbar spine can be used to integrate anatomy with the US images. The SSM is built from CT images and represents the possible anatomical variation between the lumbar spine of a given population. Intraoperative US images can be used to warp the SSM to display an estimation of the three-dimensional (3D) image of the current patient in real-time. To move towards a clinically acceptable US-guided system for percutaneous spine interventions, the objective of this thesis is to register the preoperative diagnostic CT to the intraoperative US using *in vivo* patient data. Visually, this is depicted in Figure 1.1. An accurate registration demonstrates that through the integration of anatomical information from the CT, intraoperative US is a possible image modality for needle guidance. Using US as the image modality for the guidance system will eliminate the need for intraoperative fluoroscopy or CT. The ionizing radiation exposure to the patient and physician would subsequently decrease. Additionally, CT or fluoroscopy images must be taken in protected environments due to their radiation exposure. This limits the spine interventions to specialized facilities. In contrast, US images can be taken in any location, improving the accessibility of percutaneous spine needle interventions.

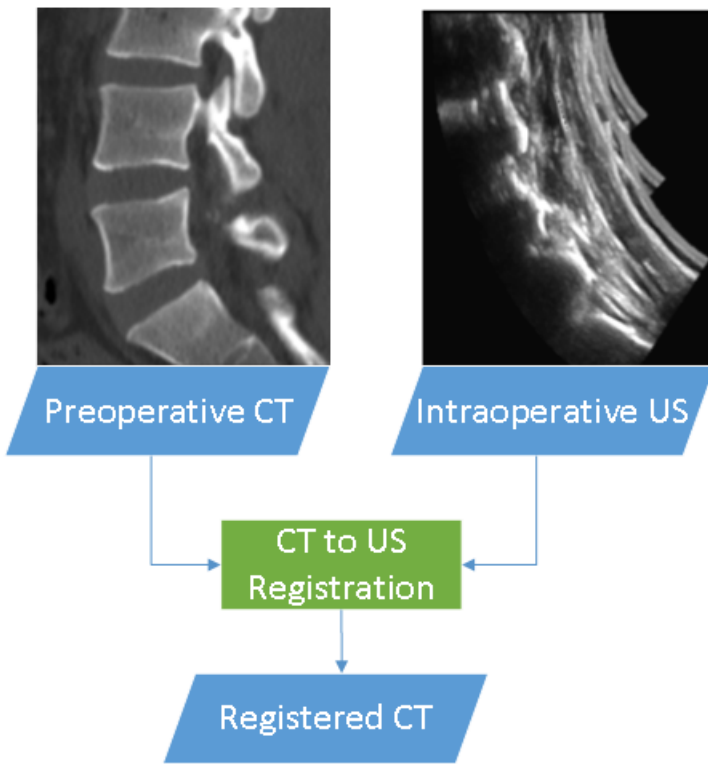


Figure 1.1: US guidance system where preoperative CT is aligned with intraoperative US.

The objective of this thesis can be divided into three goals:

1. Design a clinical US data collection protocol for the spine to decrease variability in acquired US image quality between subjects.
2. Develop an accurate and robust CT to US registration workflow for the lumbar spine that aligns the images from both imaging modalities in the presence of:
 - differing patient positioning for preoperative CT imaging and US imaging.
 - acoustic shadowing of the spine inherent to ultrasound.
3. Validate the registration approach on clinical data to determine its accuracy in a clinical setting.

1.3 Thesis Contributions

In this thesis, I have:

- Contributed to the development and testing of a protocol for US data acquisition. Assisted with the acquisition of US data from five patients using the proposed protocol.
- Created a novel registration pipeline between preoperative CT images and intraoperative US images of the lumbar spine. Bone surfaces from the CT and US images were enhanced using local phase filtering and were used as input to the registration. The registration pipeline consists of three main steps:
 - global intensity-based registration for an initial alignment.
 - global point-based registration to further align the CT and US using point correspondences in addition to the voxel information from the previous step.
 - multi-vertebrae point-based registration to correct any curvature changes between adjacent vertebrae.
- Validated the performance of the registration approach on five clinical data sets.

1.4 Thesis Outline

The thesis is organised as follows:

Chapter 2, Background: introduces percutaneous lumbar spine interventions, tracked ultrasound guidance and reviews the literature pertinent to image registration.

Chapter 3, Experimental Design: describes clinical data acquisition protocols for the preoperative CT and intraoperative tracked US, and details the validation methodology for CT to US registration.

Chapter 4, Methods: details the workflow of the registration technique involving first a global intensity-based registration, then a global point-based registration and finally a multi-vertebrae point-based registration. Any pre-processing steps on the clinical data is also explained.

Chapter 5, Results and Discussion: presents quantitative and qualitative results of the registration pipeline on the clinical data and discusses these results.

Chapter 6, Conclusions and Future Work: presents the principal outcomes of the thesis and describes potential future work that can aid with the integration of the registration workflow into a clinical setting.

Chapter 2

Background

This chapter introduces fundamental concepts for the registration of CT data to US data of the lumbar spine, and the reasoning behind performing this registration. Anatomy of the lumbar spine and needle interventions into this area are crucial to understand when developing a registration algorithm and is therefore explained in this chapter. The current CT to US registration algorithms in the literature for the lumbar spine are also explored. Finally, the available medical imaging software that is used to support this application is presented.

2.1 Percutaneous Lumbar Spine Interventions

Percutaneous spine needle injections are those that are inserted through the skin to reach their target area. Often injections of this kind are required for anesthesia or analgesia. A facet joint injection is an example of an analgesic procedure and epidural anesthesia is an example of anesthetic and analgesic procedure. Both these procedures are clinical motivations for this thesis. They are widely applied and require careful placement of the needle to reach the target area without damaging surrounding tissue and nerves. Before discussing epidural and facet joint injections,

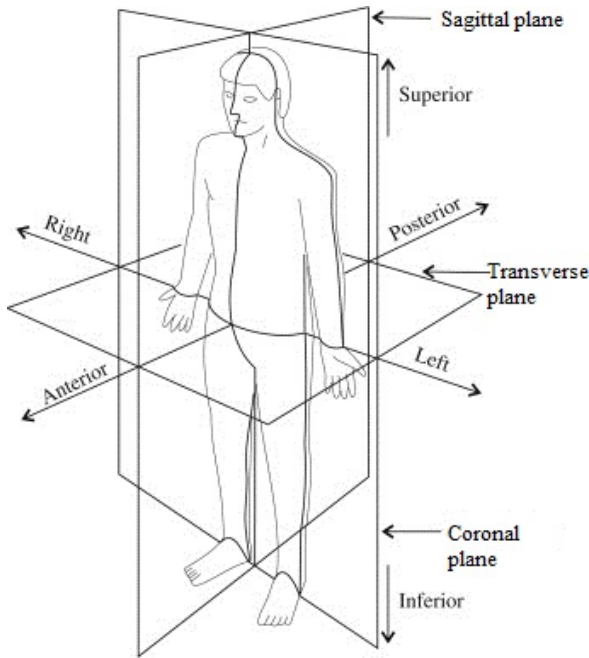


Figure 2.1: The human standardized anatomical position along with the three reference planes and six anatomical directions. This figure is modified from [48].

the anatomy of the lumbar spine relevant to these procedures is outlined.

2.1.1 Lumbar Spine Anatomy

Figure 2.1 shows the standardized anatomical position and illustrates the anatomical directions from the center of the body as well as the three reference planes: sagittal, transverse and coronal. These terms are used throughout and are important to understand before discussing the lumbar spine anatomy.

There are five lumbar vertebrae in the spine and they can be visualized in the CT sagittal slice in Figure 2.2. Two adjacent vertebrae (L4 and L5) are rendered in 3D in Figure 2.3 and annotations are added to describe the anatomy referred to throughout the thesis. A facet joint is formed between the inferior articular process

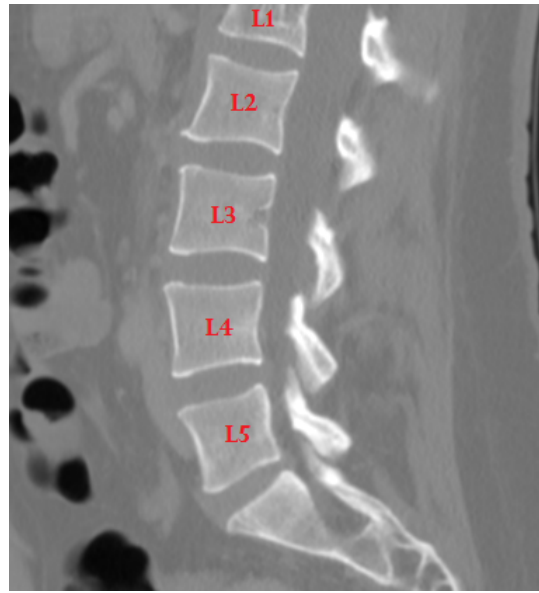


Figure 2.2: Sagittal CT slice demonstrating the five vertebrae that make up the lumbar spine.

and superior articular process of two adjacent vertebra. The lamina and spinous processes are shown and are important landmarks as they are most visible in US. The US sagittal slice in Figure 2.4 demonstrates the spinous processes in US and additional anatomy required when considering percutaneous spinal interventions. The dura surrounds the spinal cord. The posterior dura shown is between the L4 and L5 vertebrae and represents the landmark in US that can be used to guide a needle to the epidural space. The epidural space relative to the spinal cord and posterior dura is shown in Figure 2.5. Figure 2.6 demonstrates where the sagittal US slice from Figure 2.4 fits within the 3D rendering of the L4 and L5 vertebrae in the CT to provide a perspective. Figures 2.2, 2.3, 2.4, 2.5, 2.6 are all visualized using the open-source software 3D Slicer [46] [47]. This software will be described in more detail in Section 2.4.3.

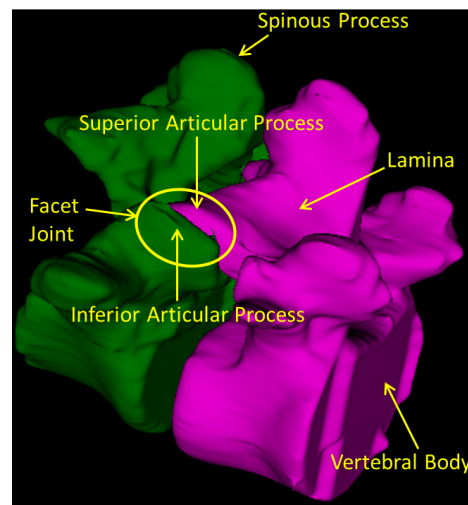


Figure 2.3: 3D rendering of the L4 and L5 vertebrae from the CT. Annotations in yellow describe various relevant spine anatomy.

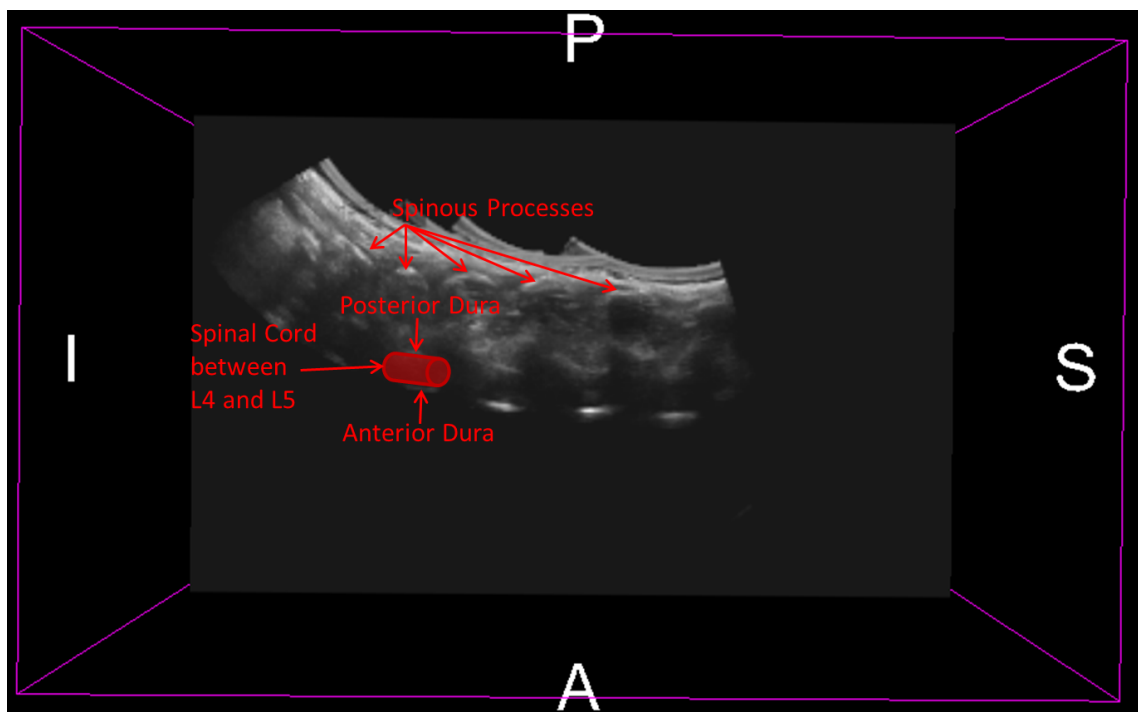


Figure 2.4: Sagittal US slice of the lumbar spine with anatomical annotations in red. The letters I, S, A, P refer to the anatomical directions inferior, superior, anterior and posterior, respectively.

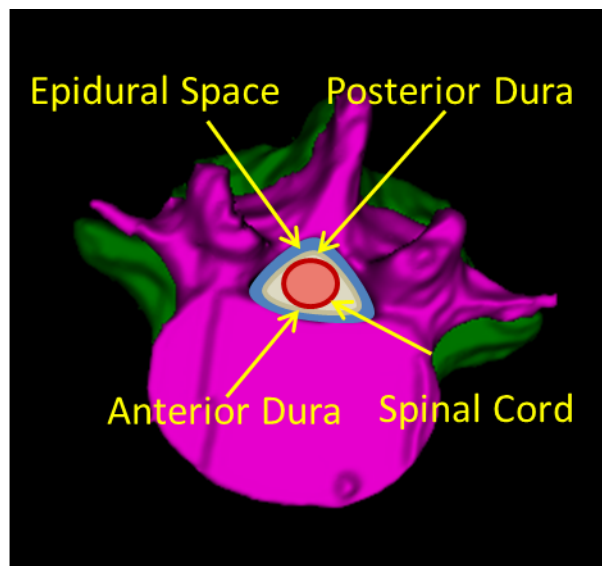


Figure 2.5: 3D rendering of the L4 and L5 vertebrae from the CT to show the location of the epidural space in blue relative to the spinal cord and dura.

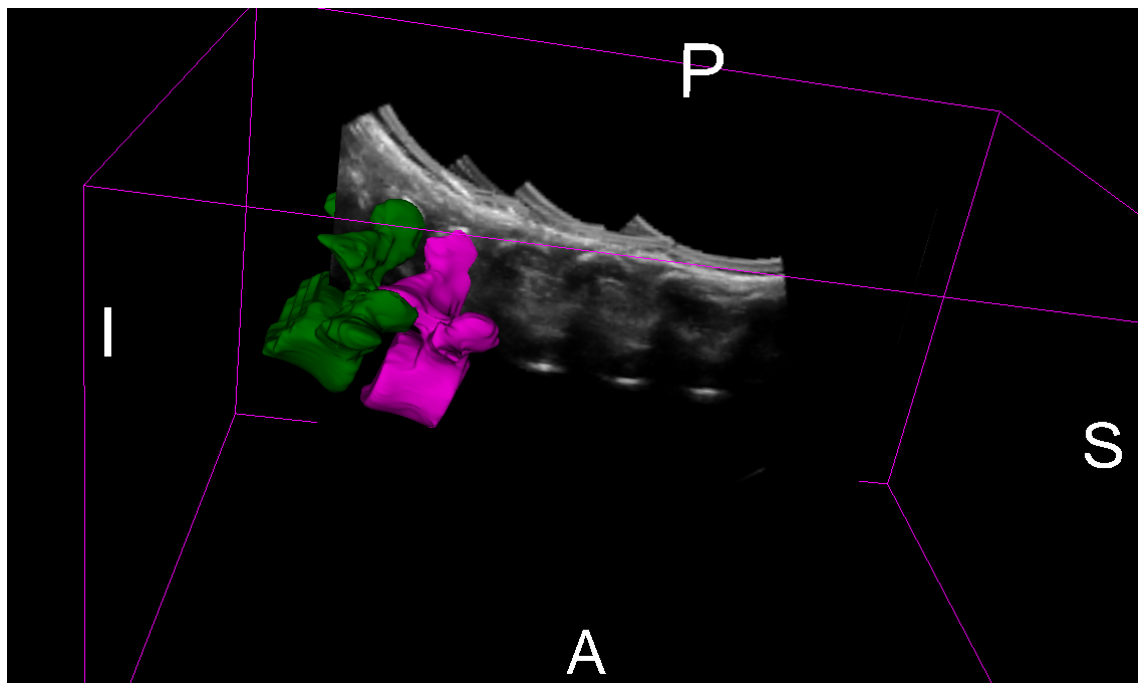


Figure 2.6: 3D rendering of the L4 and L5 vertebrae from the CT intersecting with a sagittal US plane. The letters I, S, A, P refer to the anatomical directions inferior, superior, anterior and posterior, respectively.

2.1.2 Spinal Injections

Epidural Anesthesia and Analgesia

Epidurals are delivered for surgery in place of general anesthesia [34] as well as for analgesia in obstetrics during labour [1]. Performing the procedure blindly is challenging for inexperienced anesthesiologists or when difficult cases are presented due to obesity or diseased spines [1]. In these situations, multiple insertion attempts may occur causing an increase in procedure time and discomfort to the patient [29]. In non-obstetric cases, it is possible to use fluoroscopy to guide the epidural; however, this exposes the patient and the clinical staff to ionizing radiation [27]. An example of a needle insertion into the epidural space for anesthesia or analgesia is shown in Figure 2.7. The needle enters through the space between two spinous processes. Once there is a loss of resistance when the needle penetrates the epidural space, a steroid is injected into this region. There is a risk of dural puncture if the needle is advanced through the entire epidural space and through the posterior dura [55]. Delivery to this area is challenging as White *et al.* reported that 25% of epidural injections were incorrectly placed by an experienced anesthesiologist and an orthopedic surgeon [59].

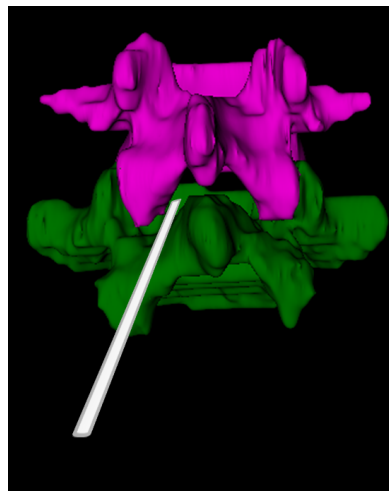


Figure 2.7: 3D rendering of the L4 and L5 vertebrae from the CT demonstrating an injection into the epidural space.

Facet Joint Injection

The facet joint has an oblique orientation relative to the sagittal plane. The oblique entry, narrow joint space and deep location make injecting into this area challenging [37]. Using CT or an anterior to posterior fluoroscopy image, the angle of needle entry is estimated based on the midpoint of the space between the two articular processes forming the joint. Depth of the needle is assessed by feel. An example needle entry into the facet joint is shown in Figure 2.8.

The facet joint causes 25 to 45% of chronic lower back pain [15]. Temporary relief is achieved through an injection of steroids into the affected joint. The gold standard for the facet joint injection is fluoroscopy or CT guidance; however, both these imaging modalities cause ionizing radiation to the patient and physicians [55].

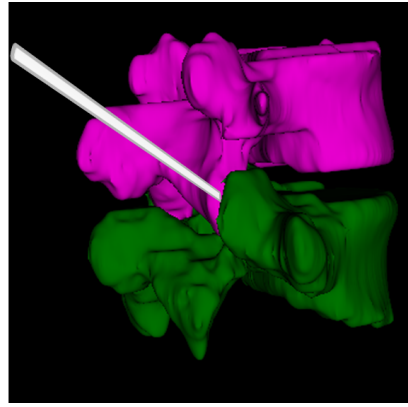


Figure 2.8: 3D rendering of the L4 and L5 vertebrae from the CT demonstrating an injection into the facet joint.

The next section focuses on the use of intraoperative US guidance for percutaneous needle interventions as an alternative to performing the procedures blindly or using ionizing image modalities, such as fluoroscopy or CT.

2.2 Ultrasound-guided Interventions of the Spine

An alternative image modality that has increased in popularity to provide guidance intraoperatively is US [41] [33]. Unlike CT and fluoroscopy, US is non-ionizing, augmenting patient safety and provides real-time guidance. It is also more broadly available and less expensive. For these reasons, US guidance for spine needle procedures will be the focus of this work.

Galiano *et al.* [18] compare the outcome of two groups receiving a facet joint injection, where one group received CT guidance and the other group underwent US guidance. They report that there was no significant difference in the outcome of the facet joint injections between the two groups [18]. Despite this promising study, US has not succeeded in replacing CT or fluoroscopy guidance. This may be due to

challenges that are inherent to the interpretation of US images for spine needle navigation. The image modality requires an experienced user having to simultaneously hold the US transducer and needle, while correctly identifying anatomy. Specifically for imaging the spine, acoustic shadowing of bone is present. This is due to a large change in the acoustic impedance between the soft tissue and bone resulting in a large reflection of the US beam at the bone surface [4]. Additionally, low frequency US transducers are commonly used to penetrate deep targets, such as the facet joint, but the deep attenuation results in a loss in the US image quality [43].

To take advantage of the benefits of US intraoperative guidance, while alleviating its limitations, the intraoperative US can be aligned to a preoperative diagnostic CT or a SSM when a CT is unavailable. Instead of using the two-dimensional (2D) US for guidance, anatomical information from the SSM or CT can be used. Without having to take an intraoperative CT, deep targets that are not seen in US can now be visualized. A SSM is built from a set of training shapes and represents the mean shape and principal modes of variations from that training set. SSM construction has been widely studied in the literature and a comprehensive review of their use in medical imaging is presented by Heimann and Meinzer [23]. The focus of this thesis is on the use of CT images to integrate anatomical information to US images for guidance.

Tracking the position of the patient intraoperatively is needed to map the preoperative CT to the patient coordinate system in which the US is taken. The electro-magnetic (EM) tracking system can be used for this purpose, and has recently gained popularity in image-guided interventions [24]. This system enables the tracking of various small EM sensors. The EM sensors can be integrated into tools, such as the

US transducer, to track its position or as stand alone sensors to provide a reference, for instance, to the patient coordinate system [62]. Given the patient coordinate reference sensor, the position of the tracked US transducer can be found relative to the patient coordinate system. Ungi *et al.* [56] developed a tracked US snapshots navigation system for facet joint injections on phantom and two lamb cadavers. However, the facet joint must be visible on the US image or snapshot to provide a specific target point that is used for guidance. In diseased spine cases where anatomy might be distorted or obesity cases where there is greater distance from the skin to the target area, visualizing a distinct target may not be possible. Instead, the information contained in the US can be augmented by the preoperative CT now that the position of the intraoperative US is known through EM tracking. The alignment of the preoperative CT to the tracked intraoperative US is referred to as registration. A brief overview of image registration between CT and US images of the spine is outlined in the next section.

2.3 Medical Image Registration

As mentioned in the previous section, the preoperative CT can be aligned to the intraoperative tracked US through the spatial mapping of anatomical structures, a process referred to as registration. Image registration was first introduced 20 years ago for use in the field of neurosurgery [45]. It has developed into a core component of medical imaging for various applications, including orthopedic surgery. Using image registration to minimize the invasiveness or reduce intraoperative radiation is important as orthopedic surgery is performed on millions of people worldwide affected by musculoskeletal disease or injury [45]. Specifically, pain associated with the spine

is the major source of chronic pain in the United States [11]. Therefore, guidance through image registration is needed to support spine interventions.

There are three main components for image registration: the optimizer, similarity metric and transformation. Registration can be thought of as an optimization problem. The optimizer maximizes or minimizes the similarity metric to determine the optimal transformation to align the two images. An example of an optimizer is one-plus-one evolutionary optimizer. This optimizer mimics biological evolution by generating random positions in the search space around the current position [25]. The similarity metric describes the degree of correspondence between the two input images and is vital to the success of a registration. One popular similarity metric is Mutual Information (MI), where images are in their optimal alignment when the amount pixel intensity information they contain about each other is maximized [14]. The transformation maps points from their original spatial coordinates of an image to new spatial coordinates of another image. The type of transformation chosen dictates the number of parameters needed to perform this transformation. Rigid transformations consist of six parameters, translation along the x,y,z directions and rotation about the x,y,z axes. Non-rigid transformations incorporate scaling and shearing and contain at least nine parameters.

There are generally two main classes of registration to find correspondence between the two images: intensity-based and feature-based. Intensity-based registration consists of the alignment of two images based on pixel intensity value similarity. Feature-based registration involves the extraction and alignment of geometric feature information common to both images, such as surface points [14]. Feature-based

registration uses sparser segmented data, while intensity-based algorithms incorporate each voxel in the volume. This means that feature-based algorithms are generally faster; however, intensity-based approaches do not require accurate segmentation and have been found to be more robust as they use all intensity information within a volume [45]. Point-based registration is a subtype of feature-based registration that finds correspondence between two point sets and is used in the proposed registration pipeline in this thesis. Current algorithms for both of intensity-based and point-based registration are explored further in the upcoming subsections. Focus is given to registration of the spine between CT and US.

2.3.1 CT to US Registration of the Spine

There exist many challenges with spine registration as the bone surface in US is noisy and shadowed, making the bone surface difficult to automatically extract. The other main challenge is the differing patient positioning between the preoperative CT, which is taken in the supine position, and the intraoperative US, which is taken in the prone or sitting position. The modification of the patient positioning between the image modalities may cause a change in the curvature of the lumbar spine. Therefore, registering the lumbar spine globally may not provide an accurate alignment. Instead, each vertebra in the lumbar spine can be treated individually as a rigid body and registered, formulating a multi-vertebrae rigid registration.

In this section, methods for automatic segmentation of the US bone surface are explored first as segmentation is often required in registrations of the spine. Next, both point-based and intensity-based approaches for CT to US registration are discussed. Where possible, focus is given to registration involving the spine. Finally,

multi-vertebrae rigid registration algorithms involving the spine are explained further within this section.

US Bone Surface Segmentation

Accurate and fast extraction and enhancement of the bone surface in US data is often needed for CT to US registration, but this remains a challenging task. The extraction of US bone surfaces is problematic due to the low signal to noise ratio and typical US imaging artifacts, such as acoustic shadowing or reverberation. Furthermore, depending on the 3D geometry of the imaged surface and the orientation of the US transducer with respect to the imaged surface, the bone surface response can be several millimeters thick. Localizing the actual bone surface within this thick response is difficult [26].

Foroughi *et al.* [17] exploit US physics to accurately extract the bone surface from US images. The method assisgns probabilities to each pixel in the US image. The probability describes the likelihood that the pixel is a part of the US bone surface. Pixels with high intensity values most likely represent bone as it is known to cause a strong reflection in US. Shadowing below this reflection is expected; therefore the combination of these two US properties is used for probability calculations. Dynamic programming is then used to minimize a cost function to determine continuity and smoothness of the bone surface. Preliminary results demonstrate that the algorithm accurately extracts bone surfaces of pelvises and femurs from US images of two cadavers.

Recently, local phase-based image processing of US has shown great promise in the automatic enhancement of the US bone surface [20] [21]. Local phase information

is contained within the frequency domain of an image. The information can be used to describe local structural features, including discontinuities. Local phase is computed in 2D through the monogenic signal, which is an isotropic extension of the one-dimensional (1D) analytic signal. The analytic signal is formed when the negative frequencies from the image signal are removed. The extracted local phase from a 2D image provides both location and orientation information of boundaries in the image [2]. This information can be used to derive symmetry-based features that represent bone-tissue interfaces in US. One of the main benefits of local phase filtering for US images is that it is invariant to differences in intensity [22]. Intensity variations are caused by US machine settings, acoustic signal loss at soft tissue and bone interfaces, and if the US transducer is not perpendicular to the imaged bone surface [30].

Local phase-based filtering has proven to be more robust for the identification of boundaries in US compared to using the intensity gradient [42]. Mulet *et al.* [39] demonstrate this by comparing their phase-based approach to identify the endocardial border to a gradient-based approach. The gradient-based approach gives equal weight to relevant and irrelevant edges, producing more noise. Since then, local phase filtering has been used in various echocardiography studies as well [42]. Similarly to the approach by Mulet *et al.* [39], Hacihaliloglu *et al.* [20] filters US images using phase symmetry features; however, the proposed method is novel in that it extracts bone.

Point-based Registration

Point-based registration finds the correspondence between two point sets and determines the transformation that maps the moving point set (CT) to the fixed point set (US). The point sets can be generated manually using fiducial landmarks or automatically extracted from the input images [38]. Ideally, point-based approaches need the following to be usable for CT to US registration of the spine: computationally inexpensive, robust to noise, outliers and missing points in one point set compared to the other point set. Missing points are expected in the US point set as the occlusion of the bone surface in US due to acoustic shadowing and orientation of the US beam is present. Noise is inherent to US and will therefore produce outliers in the point set.

The most commonly chosen point-based registration is the Iterative Closest Point (ICP) algorithm [3] [65]. At each iteration, ICP uses the closest distance between points to assign correspondences and then finds the least-squares rigid transformation by minimizing the sum of squared distances for the point sets. One major drawback to ICP is that it requires the initial alignment of the two point sets to be close [40]. Chan *et al.* [8] use ICP to register US images to a SSM for three femurs and two pelvises. An accurate US bone segmentation is needed to avoid outliers as ICP is sensitive to outliers, since it assumes equal weight to all points when computing the sum of squared distances [36]. To avoid outliers, Chan *et al.* [8] performs manual US bone segmentation, which is cumbersome. Through the manual US bone segmentation, they achieve an accuracy of less than 3.72 mm.

Moghari and Abolmaesumi [38] developed a rigid point-based algorithm that relies on the unscented Kalman filter (UKF). The UKF-based algorithm works similarly to

ICP, but there are two main differences of this algorithm: i) the algorithm processes points incrementally by sampling points according to the UKF to determine the number of points that are needed to reach convergence; ii) to account for outliers, variance information associated with the transformation parameters attained from registration is used as a confidence measure. Although improvements are reported compared to ICP, the algorithm still requires a good initial alignment [38]. The proposed algorithm is tested on a pelvic cadaver and a scaphoid bone phantom. There is 100% convergence with a mean square distance below 2 mm.

Probabilistic approaches to point-based registration were introduced to account for the limitations of methods that rely on point distances mentioned previously [3] [36] [38] [65]. Instead of enforcing a binary correspondence as in ICP, these approaches assign soft-correspondences that determine correspondences between all combinations of points according to some probability. A popular optimization approach for probability-based registration methods is Expectation Maximization [40]. An algorithm by Myronenko *et al.* [40] models the alignment of two point sets as a probability density estimation problem. One point set is represented as the Gaussian Mixture Model (GMM) centroids and the other point set is the data points. The GMM is fit to the data points by maximizing the likelihood. The parameters for probability density estimation are initially estimated during the expectation step and determined during the maximization step to update the transformation between the two point sets. Then the parameters that are found in the maximization step become the parameters specified in the estimation step in the next iteration until convergence is achieved. Testing is done on both synthetic and real point sets, including 3D face point sets. However, none of the point sets are acquired from US images. Brounstein

et al. [6] automatically extract point sets from 3D US and CT and each point set is represented as a GMM. The distance between the two GMMs is minimized during registration. The method attains a mean accuracy of 0.49 mm in a mean time of 2.12 seconds when validated on a pelvis phantom and three pelvic fracture patient datasets.

Intensity-based Registration

Intensity-based CT to US registration relies on pixel similarity between both image modalities. Unlike the point-based methods described in Section 2.3.1, intensity-based approaches do not require segmentation.

Intensity-based approaches commonly involve the use of MI for finding an optimal alignment. For instance, Johnson *et al.* [28] developed the BRAINSFit algorithm that maximizes MI from 3D images from differing image modalities. The algorithm supports rigid, and affine and B-spline deformable registration. Using MI directly on unprocessed CT and US images of the spine is not possible. CT and US images differ greatly in intensity values; therefore, intensity-based approaches often involve preprocessing the images to be more alike in terms of intensity for this type of registration.

Winter *et al.* [61] base their approach for spine registration on the fact that the brightest points in US images are generally formed from acoustic reflection of the US signal on the bone surface. The bone surface is extracted from the CT and any bone surface points that are not visible in US are removed. Then the modified CT surface and US volumes are registered based on their intensity values. The drawback of this approach is that the US transducer orientation should be known to determine what part of the bone surface is visible in US to correctly modify the CT bone surface.

Validation is done on 12 vertebrae from five patient datasets. However, only single vertebra registration is computed. This is not practical for spine needle injection guidance, since at least two registered vertebrae are needed to visualize the injection site. Yan *et al.* [63] have a similar approach to Winter *et al.* [61]; however, during the extraction of the bone surface of the CT visible in US, backward scanline tracing in addition to forward scanline tracing is performed. Again, the orientation of the US transducer is required for a robust registration. The validation is done on a plastic phantom of the spine in a water bath and a porcine cadaver. The porcine cadaver's spine is exposed and water is added to fill the cavity. This means that any soft tissue that affects visibility of anatomy in US is unrealistically removed.

The registration technique by Penney *et al.* [44] converts the pixel intensity values of both the CT and US images to create probabilistic images. At each pixel, the probability of belonging to a bone edge is determined by a probability density function (PDF). A PDF for the CT and a PDF for the US are determined through examining features, such as the intensity gradient, in training sets of CT and US images, respectively. The registration is validated on six cadaveric femurs and three cadaveric pelvises. US imaging quality is variable and depends on the subjects, operators and US machine, and the training set may not be robust in situations where bone is not as visible. Their algorithm also requires two to ten minutes for registration.

A lot of interest has been shown in approaches for spine registration where US is simulated from CT data and registration occurs between the simulated US and original US. Similarly to Penney *et al.* [44], the aim is to increase correspondence between the US and CT. Here, this is done by mapping the hounsfield units of the CT into the expected US intensity values. This was first introduced by Wein *et al.* [57] for

CT to US registration of the liver and kidney. The technique was validated on the liver and kidney of 25 patient data sets. The method was further developed by Gill *et al.* [19] for US simulation of bone. Gill *et al.* [19] successfully registers the spine of five phantom data sets and one lamb cadaver using US simulation. Simulating the US from the CT at each iteration of the registration is computationally expensive, often requiring the Graphics Processing Unit (GPU). For instance, the US simulation approach by Gill *et al.* [19] requires approximately 40 minutes on the CPU for registration.

Intensity-based registration alone does not take into account the anatomical spatial relationships when it examines intensity relationships [14]. To develop more robust registration, intensity-based approaches have been used in combination with point-based methods. Liu *et al.* [35] first uses volumetric information to initialize the registration of the cortical surface in the brain. The second step involves the use of geometric features to fine-tune the registration of the cortical surface across individuals. During the literature survey, no studies were found that combine intensity-based approaches with point-based approaches for CT to US registration of the spine.

Piecewise Rigid Registration

The spine consists of rigid vertebrae and deformable intervertebral discs between the bodies of two adjacent vertebrae. Alignment between the CT and US where possible curvature in the spine may differ requires non-rigid registration for curvature correction. Curvature correction may be needed given that the CT is taken in the supine position and US is taken in the prone position. To simplify this, multi-vertebrae rigid registration can be used. Here, the spine is divided into individual rigid registrations

for each of the vertebrae. That way, vertebrae are preserved as rigid bodies and not deformed. Cech *et al.* [7] uses this approach for CT to MR spine registration of 10 patient datasets. MI is first used to rigidly align the segmented vertebrae. Then, a deformation field is designed to rigidly transform the vertebrae, while elastically deforming the surrounding soft tissue.

The registration between CT and US by Gill *et al.* [19] uses a biomechanical model based on energy derived from the spring equation to individually transform the subvolumes of each vertebra of the lumbar spine in five phantom data sets and one lamb cadaver. The biomechanical model successfully constrains the movements of the vertebrae relative to each other during the registration. At each iteration, the subvolumes are reconstructed into a volume. The volume then undergoes US simulation. The technique is computationally expensive with a runtime of approximately 40 minutes on a CPU. It also requires manual selection of the individual subvolumes. Similarly, Rasoulian *et al.* [51] uses a biomechanical model for a multi-body unscented UKF-based registration of the lumbar spine between CT and US. Here, groups of springs are added between adjacent vertebrae to mimic the intervertebral disc. As the vertebrae are transformed, the springs' original lengths are not preserved. The springs follow Hooke's law in that the force of the spring is linearly dependent on the distance from its equilibrium length. Rasoulian *et al.* [51] validate on the same data as Gill *et al.* [19] and double the speed; however, 20 minutes is still very long for a registration.

Summary of Current CT to US Registration of the Spine

The surveyed probabilistic point-based registration methods show great potential, but have not been used for CT to US registration of the spine. Unlike ICP and UKF, a close initial alignment is not required for the success of the registration. The downside to point-based registration is that segmentation of the US bone surface is required, which is challenging. To avoid US bone segmentation, intensity-based approaches can be used. All of the intensity-based registrations discussed are only validated on phantom or animal data. Only Winter *et al.* [61] are able to register a single vertebra between CT and US using patient data. However, needle injections into the facet joint and epidural space are only possible if multiple vertebrae are registered. Biomechanical models allow registration of multiple vertebrae in phantom and one lamb cadaver; however, the methods in the literature require 20 or 40 minutes on the CPU to run. From the previous studies, a fast, robust and clinically feasible registration of multiple vertebrae is not currently available.

2.4 Medical Imaging Software

There exists various medical imaging software to support tasks in image-guided interventions. Matlab, the Public software Library for UltraSound imaging research (PLUS) software package [32] and the 3D Slicer software [46] [47] are used in this thesis and will be described briefly in this section.

2.4.1 Matlab

Matlab is a commercial software that can be used for a variety of applications, including image processing and statistics. The software also provides a programming

environment. Much of the pre-processing and registration is programmed in Matlab and details are later specified (Chapter 4).

2.4.2 PLUS

PLUS is an open-source toolkit and was created to support tracked US acquisition, calibration and processing [32]. The toolkit enables the synchronization of US image data from the US machine and tracking data from the EM tracker. Various applications from this open-source software are used to collect the tracked US data and to develop the proposed registration pipeline. A brief description of the applications is given.

Volume Reconstruction

The PLUS volume reconstructor provides the US volume reconstruction to combine the B-mode tracked US slices. Hole filling algorithms may be used within the volume reconstruction to minimize the effect of interpolation between slices during volume reconstruction.

fCal

fCal provides the GUI application for the temporal and spatial calibration of the US transducer. Prior to performing US data acquisition, calibrating the US transducer is needed because it identifies where the US image is relative to the US transducer's position.

The fCal temporal calibration is first used to automatically calculate the time offset between when the tracking data is acquired and when it is received by PLUS given

the specific hardware used. When the tracking and imaging data are appropriately synchronized to the specific hardware, spatial calibration in fCal is used to determine the US image to US transducer transformation. Spatial calibration is done by finding the correspondence between known N-wire 3D positions on a calibration phantom and the segmented wire positions in the US image [32]. Once the US transducer is calibrated to the specified depth, fCal produces a configuration file with the US image to US transducer transformation.

2.4.3 Slicer

Another open-source software package that is used extensively in this thesis is 3D Slicer, which is built on the Insight Toolkit (ITK) and the Visualization Toolkit (VTK) [46] [47]. The software provides visualization and analysis of medical images, including segmentation and registration.

All of the visualization of US and CT images presented in this work are taken as screenshots of the 3D Slicer software. The three anatomical planes are used to display CT and US slices and 3D rendering is used for the CT volume.

Various registration algorithms based on ITK, including rigid and non-rigid are available. The module General Registration (BRAINS) that employs the BRAINS-Fit algorithm [28] is used for the intensity-based registration step in the proposed registration pipeline.

Another feature within the 3D Slicer software that is used in this work is the Python Qt-based console that provides access to the VTK, Qt, and 3D Slicer wrapped APIs [46] [47]. Images can be analyzed or modified in real-time. Points are labeled according to the vertebra they belong to using this Python console within 3D Slicer.

All of the validation is done in the Python console as there is access to the CT to US registration transformations and landmark points to calculate the TRE.

2.5 Summary

This chapter introduced the percutaneous needle interventions and challenges present with the current clinical practice. Tracked US offers an alternative to blind or ionizing image modalities. Approaches in image registration for the spine were presented. Currently, there is no robust algorithm to register clinical CT and US data of multiple vertebrae in the lumbar spine. Only one study used clinical data; however, only single vertebra registration was achieved. To guide percutaneous spine needle injections, registration of at least two vertebrae are needed to visualize the injection site. All of the other registration algorithms presented in this chapter for the spine validated their registration algorithms on phantom or animal data. Finally, the medical imaging software that was used to support the development of the registration pipeline in this thesis was specified.

Chapter 3

Experimental Design

Human data sets of the lumbar spine are used to validate the proposed registration algorithm. The accuracy achieved by registration is highly dependent on the quality of the acquired US images. Therefore, a protocol is created to set guidelines for US imaging parameters and the freehand US data acquisition. The aim of the protocol is to minimize variability in US image quality between subjects, operators and imaging centres. The protocol also ensures that the setup time is minimal to adhere to the current clinical practice. Validating the registration pipeline on patient data determines whether preoperative CT to intraoperative US registration is clinically feasible. Five patient data sets acquired by a trained sonographer are used for validation.

In this chapter, the data acquisition system for the preoperative CT and intraoperative tracked US data is described. The protocol for tracked US is also detailed. Finally, the validation used to test the registration algorithm is explained.

3.1 CT Data Acquisition

Preoperative CT data were collected at St.Paul's Hospital, Vancouver, BC. Approval was obtained from Institutional Research Ethics Boards (IREB). Informed consent

Table 3.1: Demographics of subjects recruited for US imaging.

Dataset	Sex	Age	Weight (pounds)	Height (cm)
Patient 1	Female	28	158	167
Patient 2	Female	46	202	172
Patient 3	Female	49	135	178
Patient 4	Female	33	140	173
Patient 5	Male	33	171	168

was acquired from the subjects that participate in the study. Only subjects with previous CT scans were recruited to avoid any unnecessary radiation exposure. The demographics of the five subjects recruited are shown in Table 3.1. The CT images were provided as anonymized DICOM files from the hospital archiving systems. The patient is in the supine position during the acquisition of the CT data. Often, their CT only contained a small portion of their lumbar spine.

3.2 Tracked US Data Acquisition

A protocol is designed to help with the acquisition of tracked US data for the CT to US registration problem. The protocol aims to minimize variability in image quality across all subjects, imaging centres and US operators. The system used for tracked US image collection consists of both hardware and software components. The protocol describes the hardware, software and patient setup for tracked US data acquisition. The details of the US imaging are also outlined in the protocol.

3.2.1 Hardware Setup

The hardware used to acquire the US images and associated tracking data is composed of a SonixTouch US scanner (Ultrasonix, Richmond, BC, Canada) with a Guidance Positioning System (GPS) extension (Ascension DriveBay EM position tracker, Burlington, VT) and a C5-2 GPS curvilinear US transducer (Ultrasonix). Finally, a Model 800 EM tracking sensor (Ascension) is used as the patient coordinate reference. This reference sensor is affixed on the patient’s skin above the T12 vertebra, which is within its operating range (78 cm) for scanning the lumbar vertebrae [13]. The GPS extension has an adjustable arm that attaches to the US machine. This allows the position of the EM transmitter to be as close to the reference sensor as possible. The US transducer is tracked by the EM transmitter through an embedded pose sensor. A schematic of the hardware setup for the data acquisition system for tracked US is seen in Figure 3.1. The setup time is minimal (around five minutes) in order to adhere to the clinical environment and avoid any changes to the current clinical practice.

3.2.2 Software Setup

The software component comprises of the freely available and open-source PLUS toolkit [32]. The toolkit and the components used are described in Section 2.4.2. PLUS enables the synchronization of the US image data from the US machine and tracking data from the EM tracker.

Before the US data acquisition, the US transducer is calibrated using fCal for depths between 6 cm and 9 cm. A brief description of the calibration and fCal is discussed in Section 2.4.2.

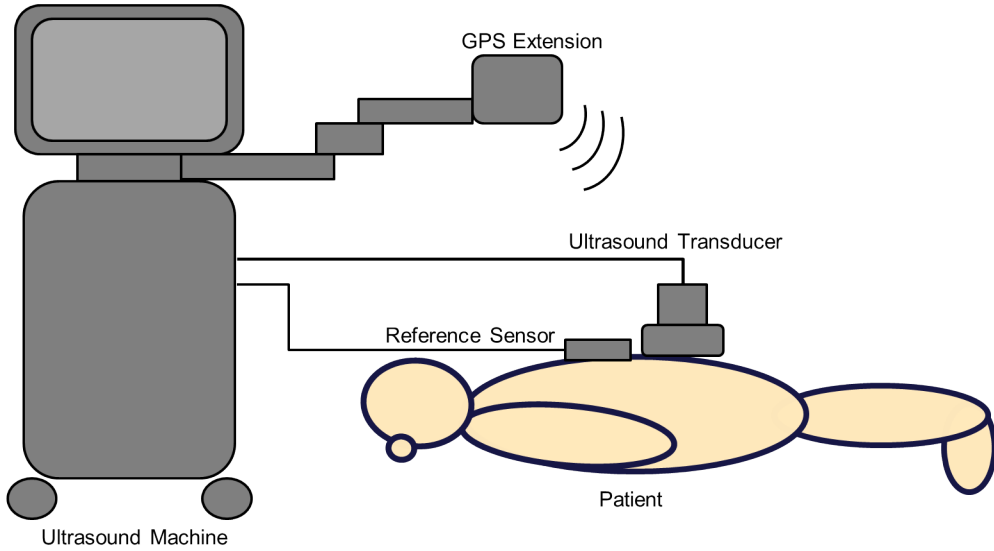


Figure 3.1: Data acquisition system for tracked US. SonixTouch (Ultrasonix, Richmond, BC) ultrasound scanner; GPS extension (Ascension DriveBay electromagnetic tracker); tracked C5-2 curvilinear transducer (Ultrasonix); 3D position sensors affixed to the transducer and patient. This figure is modified from [56].

fCal is also used for the tracked US data acquisition of subjects. For each subject, the amount of tissue between the skin and the spine differs so the depth of the US transducer needs to change to be able to visualize the spine anatomy in US. Once an appropriate depth is selected by a trained sonographer, fCal connects to the hardware using the configuration file associated with the depth chosen.

3.2.3 Patient Setup

Subjects are set in the prone position. Curvature of the spine may vary as the CT is acquired in the supine position and the US is acquired in the prone position. To help minimize a possible change in curvature between the CT and US, a medium-sized pillow is placed under the subject's stomach during the US data acquisition. The



Figure 3.2: Volunteer demonstrating the subject’s position during the US data acquisition. The subject is in the prone position with a pillow under their stomach.

positioning of the subject is visualized in Figure 3.2.

The sonographer then begins to scan the subject and adjusts the US imaging parameters, such as depth, based off of a preset of US imaging parameters. The preset was first created alongside the sonographer based on US images of volunteers. Only minor manual adjustments to the imaging parameters for each individual are needed to reduce intraoperative time.

The sonographer then landmarks the T12 vertebrae and sacrum as well as the ends of the L1 transverse processes to determine the US scanning region. This ensures that the entire lumbar region of the spine is scanned. The reference holder is attached approximately 3 cm above the T12 vertebra landmark. The reference sensor that acts as the patient coordinate reference is placed into the reference holder. The reference holder is depicted in Figure 3.3 and orients the reference sensor such that the patient coordinate frame matches the anatomical directions of the patient described in Section 2.1.1.

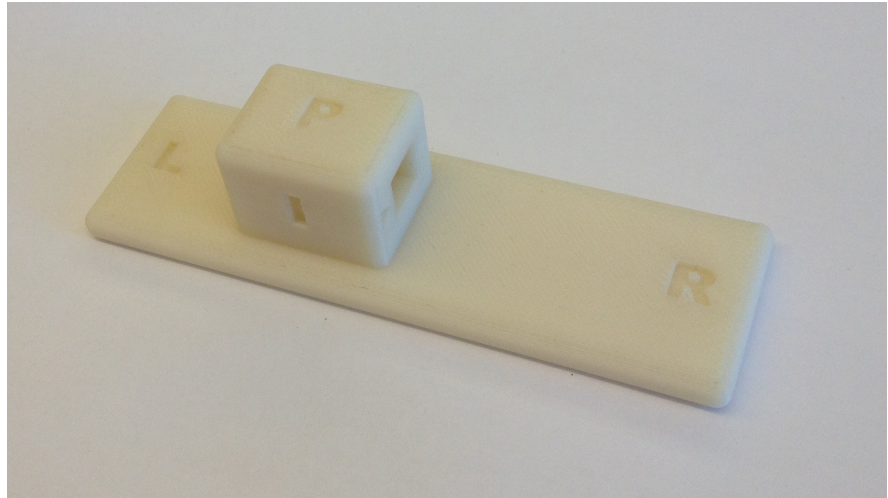


Figure 3.3: Reference sensor holder that orients the reference sensor according to the anatomical directions.

3.2.4 US scanning

During the US data acquisition, an US scan is completed in a minimum specified time to ensure the US transducer moves slowly and smoothly, while keeping complete contact between the subject's skin and the ultrasound transducer (minimum of twenty seconds). By moving slowly, more 2D US images are acquired during the US scan. This decreases the degree of interpolation needed during the 3D volume reconstruction of the 2D US images and consequently improves the US volume's image quality for CT to US registration. US volume reconstruction was described in Section 2.4.2.

It was evident from the initial ultrasound scans of volunteers that the curvature of the spine varies between individuals. For this reason, three different scan styles in both the transverse and sagittal directions are designed to ensure that at least one scan provides good quality US images. The following are the three types of scans performed for each subject:

- transverse U-shaped scan: the US transducer starts at the top of the L1 vertebra

and slightly off to the left of the midline then moves down and when it reaches the sacrum, the US transducer moves slightly to the right of the midline and back up to L1. This scan style identified the deep targets, such as the facet joint the most clearly.

- transverse midline: the US transducer starts at the top of the L1 vertebra and moves straight down the midline until it hits the sacrum. Moving the US transducer straight down the midline may prevent the imaging of the full width of a vertebra by excluding the transverse processes.
- sagittal zigzag: the US transducer starts at the left L1 transverse process and moves across to the right L1 transverse process. It then moves down and across in the opposite direction to acquire US image of the entire lumbar spine. This scan style reliably shows the lamina and is chosen for the proposed registration workflow.

For each scan style, example US images with annotations and a schematic of the scan style are shown in Figure 3.4.

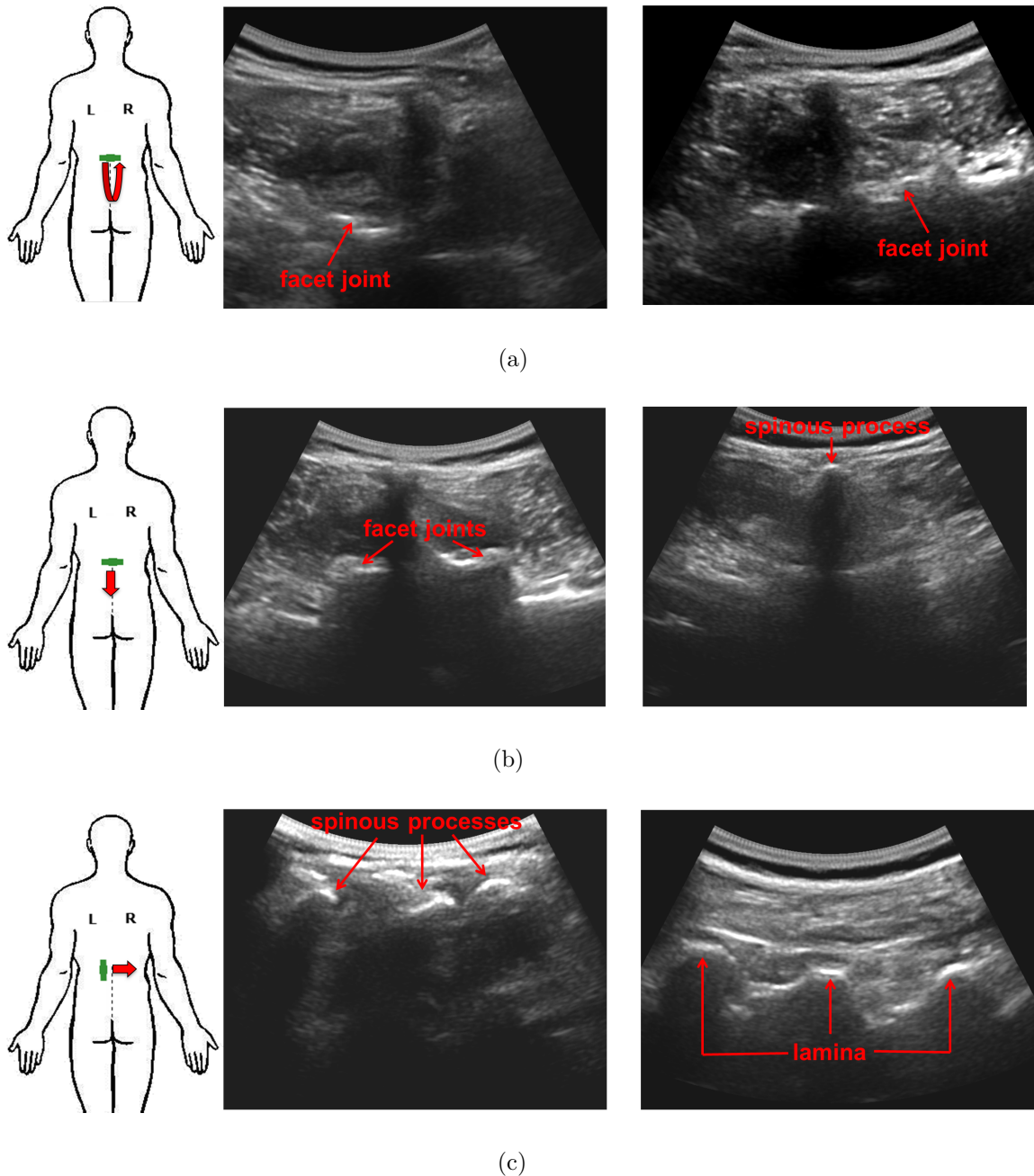


Figure 3.4: Scan styles for US data acquisition with example US images. Annotations of anatomy are shown in red.(a) transverse U-shaped scan; (b) transverse midline scan; (c) sagittal zigzag scan.

3.3 Validating the Alignment of the US and CT Images

Quantifying the accuracy of the CT to US registration is difficult due to the lack of a gold standard. A gold standard consists of a set of known, corresponding points called fiducial markers that are visible in both the US and CT images. Corresponding points in the CT and US images can then be matched and deviations from the optimal alignment following registration can be calculated.

A gold standard alignment is not possible for the five patient data sets used in this work for validation as recruited subjects already have CT scans available. Since the CT scans are previously acquired, fiducial markers that are visible in both CT and US cannot be used. In place of a gold standard, anatomical landmarks on the lamina of each vertebra are placed on the US images. Two operators choose these anatomical landmarks: one orthopedic surgeon and one MD with spine anatomy expertise. The landmarks chosen by the two operators are pooled together. An F-test is performed based on results from one patient ($F = 0.98$) and interoperator variability is not found to be significant. In the absence of fiducial markers, we assume the CT and US have the optimal alignment following registration. The landmarks points chosen in US are assumed to correspond to the same landmarks in the CT and are visually confirmed.

To determine the accuracy and precision of the registration method, the CT and the points representing the lamina landmarks are perturbed by a transformation selected randomly from a uniform distribution of 5° rotation about each axis and 5 mm translation along each axis. The transformation is applied to the entire lumbar spine that is visible in the CT.

The initial misalignment is determined by calculating the target registration error

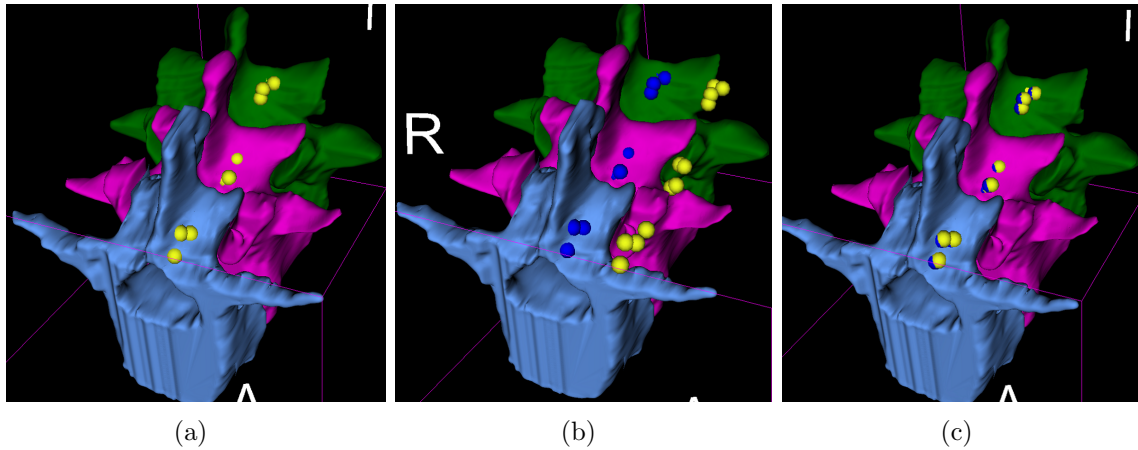


Figure 3.5: One case of quantitative validation of the CT to US alignment using lamina landmarks placed on the US. Original positions of landmarks are shown in yellow after the alignment of the CT to the US and the transformed positions are shown in blue. (a) CT aligned to original position of US lamina landmarks; (b) CT and lamina landmarks transformed by initial perturbation; (c) CT and lamina landmarks transformed by CT to US transformation found through registration pipeline.

(TRE) between the original position of the lamina landmark points and the position of the landmarks after the initial perturbation. To determine the capture range for the registration pipeline, 20 tests are performed with misalignment errors randomly generated within the range 0 - 25 mm.

Registration is then performed and the final TRE is calculated as the root mean square between the transformed lamina landmark points and their original positions. One test run out of the 20 for one subject is shown as an example in Figure 3.5 to demonstrate how this validation works pictorially.

A qualitative clinical validation is also investigated. Here, a point is added on the posterior dura between two adjacent vertebra in the US images by both operators. This is where the clinician aims their needle for spinal anaesthesia and thus provides a clinically relevant validation [9]. If the points selected are in the correct region, as

seen in Figure 3.6, after registering the CT to the US, the registration is potentially suitable for spinal anesthesia.

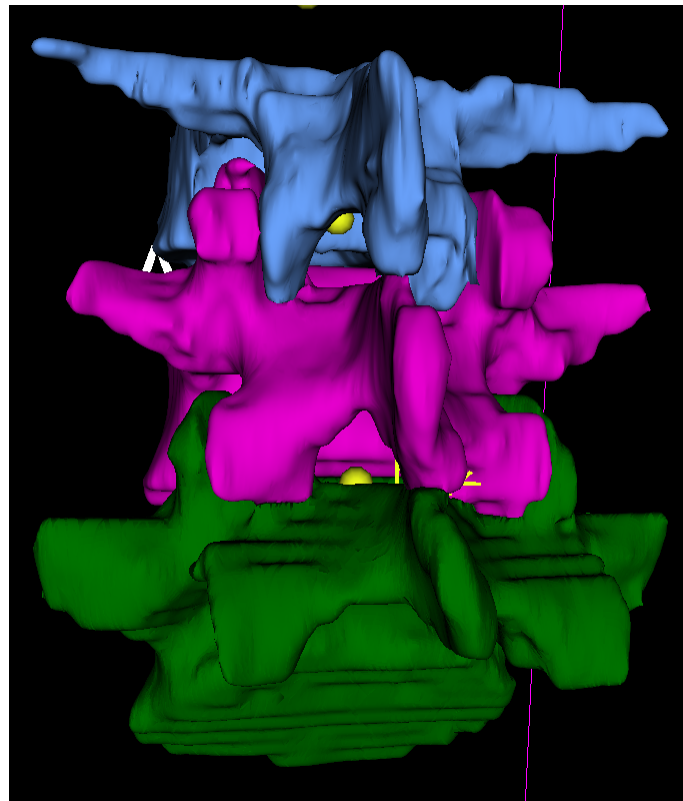


Figure 3.6: One case of qualitative validation of the CT to US alignment using posterior dura landmarks on the US signifying where a needle's target would be for spinal anesthesia. Landmarks are shown in yellow.

3.4 Summary

This chapter explained how the patient preoperative CT data and the intraoperative tracked US data were collected in order to validate the proposed registration pipeline on five clinical datasets. The protocol described all aspects of the US acquisition preparation, including the hardware, software and patient setup. The details of the setup help to ensure that the data acquisition runs smoothly and quickly to work

within a clinical environment. Guidelines for data acquisition were also discussed, such as scan styles. These guidelines help control the quality of the spine ultrasound images that are needed for a CT to US registration. The methodology used for validating the clinical CT to US registration was also presented. Details on how the acquired CT and US data are used in the registration pipeline is discussed in the next chapter.

Chapter 4

Methods

The previous chapter discussed the process of acquiring the clinical preoperative CT and intraoperative tracked US data. This chapter presents the registration pipeline used to align these acquired datasets. Registration of the preoperative CT to the intraoperative US provides a 3D visualization of the patient's specific anatomy without having to perform CT or fluoroscopy intraoperatively.

The low signal to noise ratio and acoustic shadowing inherent to US are examples of why the US and CT image differ greatly. These differences prevent the direct registration of the CT volume to the US volume without the need for preprocessing. The proposed methodology requires preprocessing of each of the volumes to automatically enhance the bone surface. The enhanced bone surfaces are used as inputs to the registration pipeline.

The registration pipeline involves both intensity-based and point-based registration of the bone surfaces to harness the advantages of each method. The aim of the registration workflow is to maximize the similarity using both voxel information and features (points) extracted from the input volumes to find the closest alignment between the CT and US. The general overview of the registration pipeline is illustrated

in Figure 4.1. The approach can be divided into the following three major steps:

1. **Automatic global intensity-based registration to align the CT and US using voxel information.** The algorithm used is a module in the open-source medical imaging software 3D Slicer [46] [47] (Section 2.4.3). The parameters, including the center of geometry initialization, are chosen to achieve the best possible alignment. The intensity-based registration module is chosen for the first step of the pipeline as it is readily available in 3D Slicer [46] [47]. Although it was developed for multi-modality registration for the brain, it is used successfully for a variety of multi-modality applications [16] [28]. Local phase bone features are automatically extracted from both CT and US data sets using the novel approach developed by Hacihaliloglu *et al.* [22]. Local phase is used to enhance the US bone surface as it is invariant to intensity changes that are common to US imaging.
2. **Automatic global point-based registration using solely point set correspondences.** An existing point-based registration algorithm called Coherent Point Drift (CPD) developed by Myronenko *et al.* [40] is used. The CPD algorithm is used as probabilistic point-based approaches are generally more robust to noise, outliers and a close initial alignment. The approach shows promise for CT to US registration of the lumbar spine as it was also used previously for SSM to US registration of the spine [50]. Modifications are made to an existing US bone surface segmentation used for this step to reduce the amount of noise [17]. The algorithm by Foroughi *et al.* [17] is modified since it provided accurate US bone segmentations given human cadaveric US data and is expected to translate well to human US data.

3. Novel automatic multi-vertebrae point-based registration to account for possible curvature changes of each vertebra along the lumbar spine. Here, the CPD algorithm [40] is modified to perform a multi-vertebrae rigid registration. Preoperatively, artificial springs are chosen between adjacent vertebrae to constrain the movement of the individual rigid bodies (vertebra). Automatic labeling of each vertebra is also performed preoperatively. The labels used come from an automatic segmentation by Rasoulian *et al.* [52]. This step is included as previous multi-vertebrae registration algorithms demonstrate that individually transforming the vertebrae corrects any curvature changes between the CT and US data [19] [51].

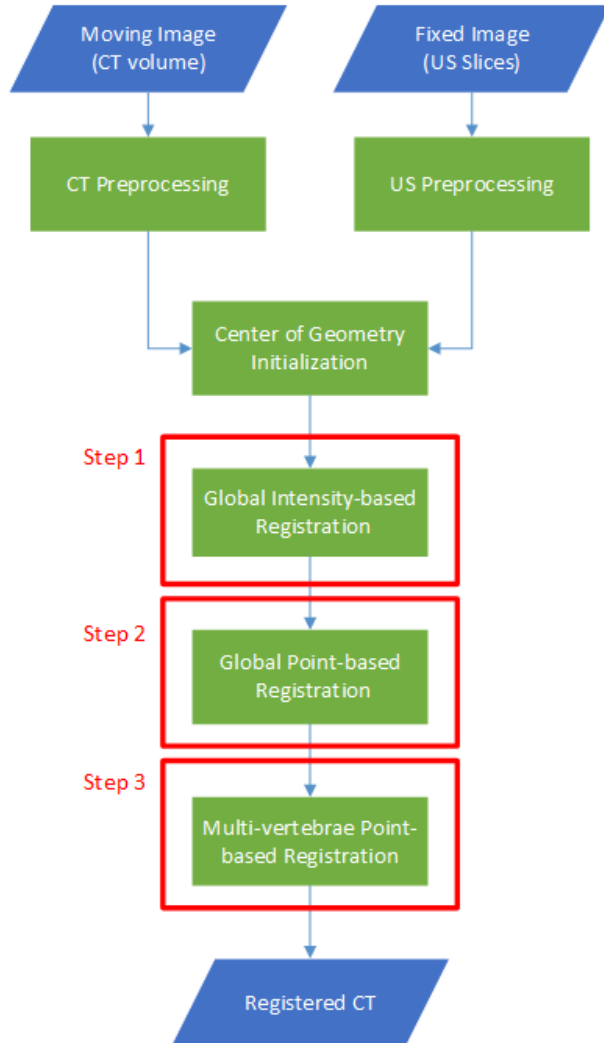


Figure 4.1: General overview of the CT to US registration workflow.

Each of these steps are explained in detail in the subsequent sections.

4.1 Global Intensity-based Registration

Global intensity-based registration is used as step 1 in the registration pipeline. In order to perform the registration between the CT and US, preprocessing of the images from both modalities is necessary. Details of the preprocessing steps required

are summarized in Figure 4.2, which is expanded from the general overview of the registration pipeline seen in Figure 4.1. As mentioned in Section 2.3.1, the images from a CT and US differ greatly, especially in terms of intensity values. Given an intensity-based registration, where correspondence is found through the voxel values, the preprocessing must eliminate the variability of the intensity values in the CT and US images as much as possible. Local phase filtering is used to automatically enhance the bone surface from both the CT and the reconstructed US volume. Only the CT bone surface visible in the US is used to avoid intensity values that would not exist in US imaging. The local phase filtering is programmed in Matlab by Hacihaliloglu [22]. The processed volumes are then provided as input to a built-in intensity-based General Registration (BRAINS) module [28] in the open-source software 3D Slicer (Section 2.4.3) [46] [47]. Details of the filtering used to automatically enhance the bone surfaces, while eliminating soft tissue in the CT and US, respectively, are presented next.

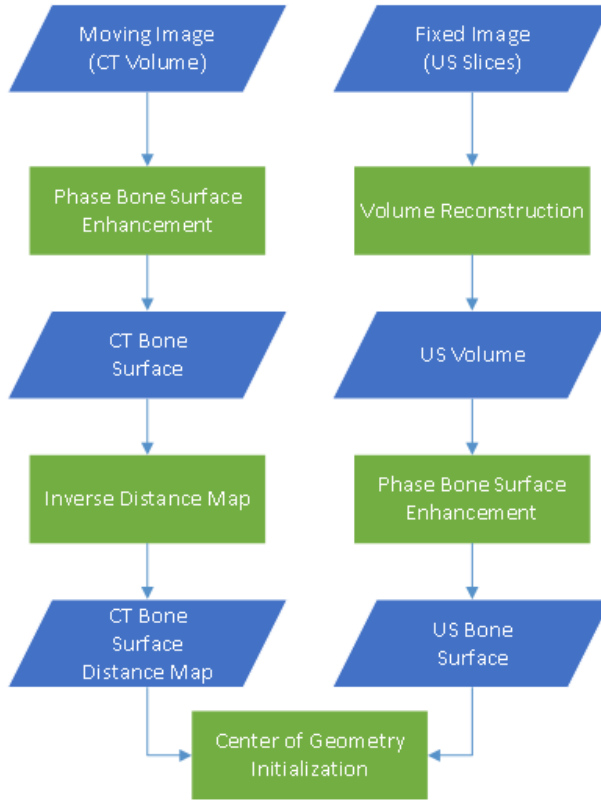


Figure 4.2: Expansion of Figure 4.1 to show details of the preprocessing for the intensity-based rigid registration.

4.1.1 Phase-based CT Bone Surface Segmentation

To automatically enhance the CT bone surface, the CT is filtered in the frequency domain using local phase image processing. The frequency domain provides local amplitude and local phase information about an image signal. Local amplitude describes the local strength of the image signal and the local phase represents the local structural features, such as discontinuities.

The 1D analytic signal is a representation of the image signal where negative frequencies are removed to be able to compute local phase and local amplitude. The monogenic signal provides an isotropic extension of the analytic signal concept to

higher 2D or 3D dimensions. Typically, access to these local properties in 2D and 3D is accomplished through the construction of a quadrature pair of oriented band-pass filters. These filters are a 90 degree phase shift version of each other [49]. The Log-Gabor filter is used as the band-pass quadrature filter on the CT slices. It is chosen as it is also used for local phase filtering of the US (Section 4.1.2).

CT local phase filtering (CTP) uses a combination of the local amplitude (A) and local phase (ϕ) and is given by:

$$CTP = A \times \cos(2 \times \phi) \quad (4.1)$$

CTP extracts a single feature, the step edge, which corresponds to a sharp change in the intensity of an image. Step edges occur at a soft-tissue to bone interfaces as the appearance of bone is significantly brighter than soft-tissue.

A simple raycasting is done following the (CTP) phase filtering in the posterior to anterior direction such that the first bone pixel encountered for each column is saved as bone and anything below that pixel is saved as background. The raycasting helps to remove the bright intensity values that exist in CT, but do not exist in US, since US signals cannot propagate through the bone surface. A sagittal CT slice from two different patients overlaid with the local phase bone surface enhanced from the CT followed by the raycasting are seen in Figure 4.3. The inverse Euclidean distance map is calculated on the enhanced bone surface CT image by calculating the Euclidean distance between each pixel and the nearest non-zero pixel of the image. The inverse Euclidean distance is used so that as the distance increases from the CT bone surface, the intensity values decrease. Thus, the intensity values at the bone surface are maximized. The inverse distance maps of the enhanced CT bone surface

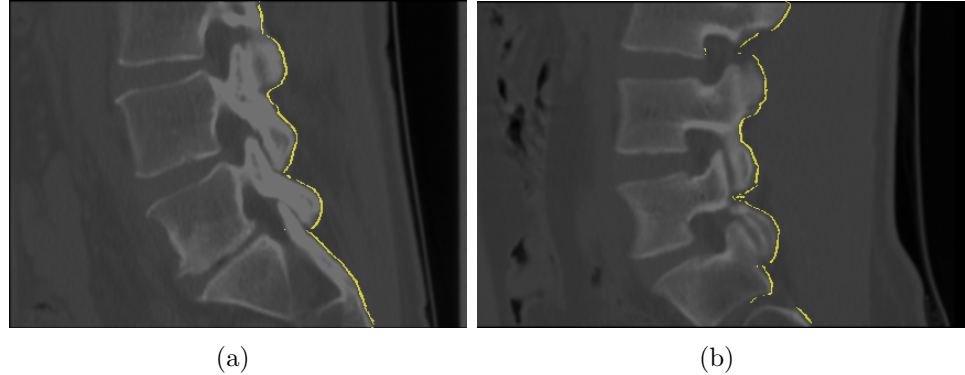


Figure 4.3: Sagittal CT slice overlaid in yellow with the phase filtered and raycasted bone surface. (a) CT slice from patient 3 with its corresponding raycasted bone surface. (b) CT slice from patient 5 with its corresponding raycasted bone surface.

corresponding to Figure 4.3 are depicted in Figure 4.4.

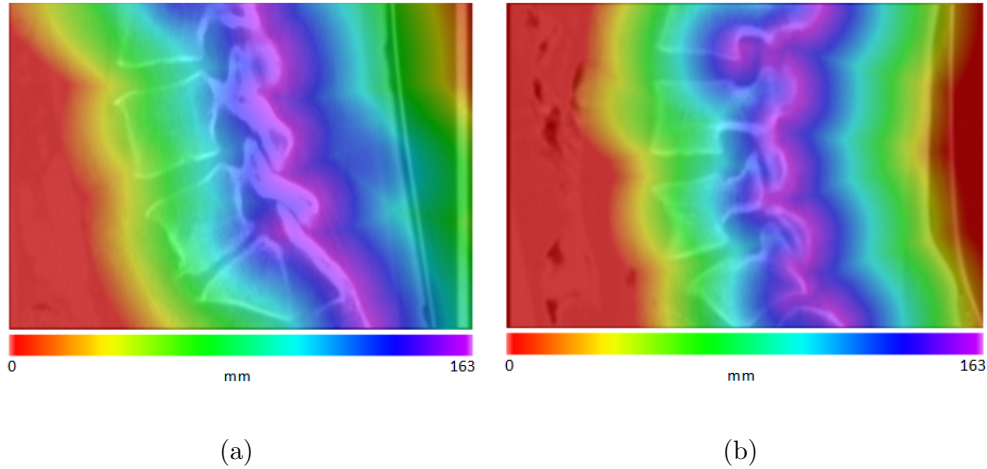


Figure 4.4: Sagittal CT slice overlaid with the inverse Euclidean distance map of the enhanced bone surface. (a) Inverse distance map corresponding to the bone surface in Figure 4.3(a). (b) Inverse distance map corresponding to the bone surface in Figure 4.3(b).

Local phase filtering is chosen to extract the bone surface from the CT to enhance the similarity between the CT and US, since local phase filtering is also used to extract

the bone surface for the US volumes as described in the next section (Section 4.1.2). Methods that simulate US from CT [19] [54] [57] follow a similar concept in that they also change the CT to contain similar features as the US. However, compared to approaches involving simulating US from a CT, local phase processing of the CT volume is much less computationally intensive [31].

4.1.2 Phase-based US Bone Surface Segmentation

The B-mode 2D ultrasound slices are reconstructed using the volume reconstructor in the open-source PLUS library. A brief description of volume reconstruction is found in Section 2.4.2. Following volume reconstruction, the local phase features are extracted from the US reconstructed volume to automatically enhance the US bone surface relative to the soft tissue. The local phase filtering approach was developed by Hacihaliloglu *et al.* [22].

The US local phase filtering differs from the outlined CT local phase filtering (Section 4.1.1). The CT local phase filtering extracts only a single type of feature (step edge), while the US requires multiple features (step edge, line, corner, junction) due to the complex shape of vertebrae in US. Rather than assuming one orientation as is done in the CT local phase filtering (Section 4.1.1), the US local phase filtering allows for the simultaneous estimation of the orientation and local phase information [22].

Similarly to the CT local phase filtering (Section 4.1.1), the US B-mode images are filtered by the Log-Gabor band-pass quadrature filter to access the local phase and local amplitude from the monogenic signal. The Log-Gabor filter is chosen as it is widely used in image processing of bone and soft tissue interfaces in US [22].

The phase metric called the local phase tensor (LPT) combines local amplitude

(A) and the local phase that extracts multiple features (ψ) [22]. LPT is given by:

$$LPT = A \times \cos \psi \quad (4.2)$$

The extraction of multiple features allows the LPT metric to behave as a general boundary indicator providing improved local phase responses.

Raycasting is then done following the (LPT) filtering from the anterior to posterior direction in order to remove any soft tissue visible above the bone signals. For each column, the first occurrence of bright intensities is found and this phase information is kept, excluding most bright pixels accidentally found during the phase filtering in the soft tissue. The raycasting direction did not need to change for each patient as the reference holder in Figure 3.3 ensures that the US data is oriented according to the human anatomical directions. A sagittal US slice of two of the patients with enhanced bone surface overlaid is shown in Figure 4.5. For registration, the number of vertebrae in the CT scan should be the same as the number of vertebrae in the US volume. For this reason, a region of interest of the US is selected that corresponds to the portion of the lumbar spine visible in the CT.

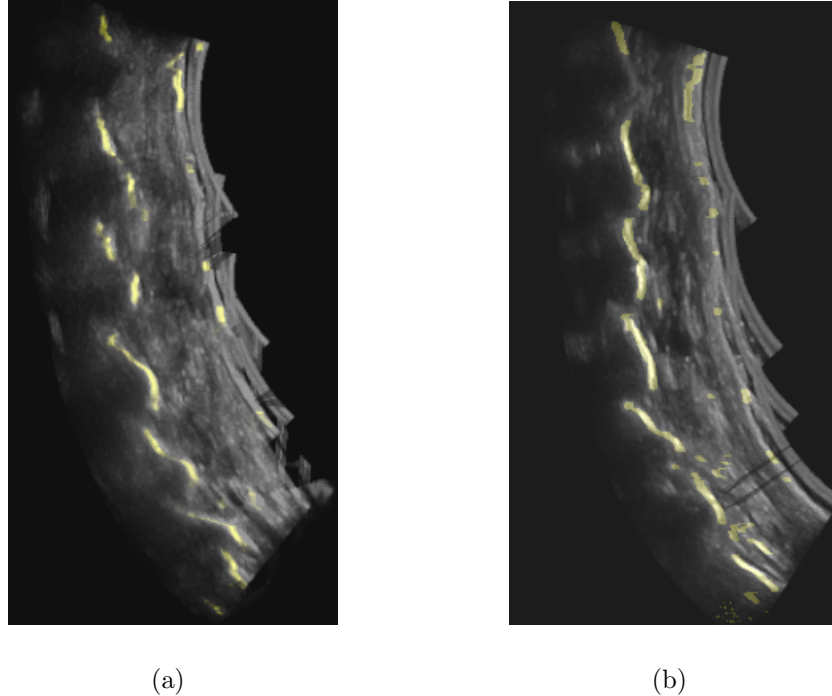


Figure 4.5: Sagittal US slice. The phase filtered and raycasted bone surface is overlaid on the US slice and is shown in yellow. (a) US slice from patient 3. (b) US slice from patient 5.

4.1.3 Rigid Phase CT to US Registration

3D Slicer as described in Section 2.4.3 is used to automatically register the preprocessed CT to the preprocessed US using an intensity-based approach [46] [47]. The General Registration (BRAINS) module within 3D Slicer version 4.2 that employs the BRAINSFit algorithm is used [28]. MI is used as the similarity metric for registration. Optimal alignment is achieved when the amount of pixel intensity information each input image contains about each other is maximized. The module's default parameters are used to run the registration unless specified. The registration is initialized given

the transformation of the center of geometry of the preprocessed CT volume (Section 4.1.2) to the center of geometry of the preprocessed US volume (Section 4.1.2). This assumes that the center of geometry in both image modalities represent similar structures. The rigid transform option is selected in order to perform a rigid intensity-based registration. Six parameters are optimized representing the translations in each x, y, z direction and the rotation in each x, y, z direction to apply to the CT. This completes the first step to align the CT to the US.

4.2 Global Point-based Registration

To fine tune the global intensity-based registration (step 1), step 2 and step 3 involve point-based registration, where step 2 performs a global point-based registration and step 3 utilizes a novel multi-vertebrae point-based registration. The rigid component in both steps uses the CPD point-based registration algorithm developed by Myronenko *et al.* [40].

For both step 2 and step 3, the CT point set is obtained from the CT bone surface that was discussed in Section 4.1.1. One additional processing step is needed for the CT point set for step 3, where the points are automatically labeled based on the vertebra they belong to in order to transform each vertebra individually for the multi-vertebrae point-based registration. Preprocessing of the US used for both step 2 and step 3 is outlined next. A more detailed description of the CPD algorithm and the multibody CPD algorithm is explained in the upcoming subsections. The US bone segmentation, CPD and multibody CPD implementations are done in Matlab.

4.2.1 Single Pixel US Bone Surface Segmentation

The local phase US filtering (Section 4.1.2) cannot be used for the point-based registrations as it enhances the US bone surface, but does not segment it. The segmented US bone surface is needed to perform a point-based registration. An algorithm by Foroughi *et al.* [17] is used to automatically extract a single pixel bone surface from the US. In the original algorithm, the US images are initially smoothed using Gaussian filtering to reduce speckle from the US. The bone surface pixels are then enhanced by a combination of two main bone features: high acoustic impedance and acoustic shadowing. Due to the high acoustic impedance of bone in US, a pixel that is most likely bone will have a high intensity value, since there is a strong reflection when the US beam hits a bone surface. Due to this reflection, acoustic shadowing should also be present below the bone. Pixels with low intensities are therefore expected below a pixel of high intensity if the pixel of high intensity is a part of the bone surface. Continuity and smoothness of the bone surface are established by minimizing a cost function using dynamic programming [17].

Foroughi *et al.* [17] tested their algorithm on ultrasound data from cadavers. Since the data used in the presented registration pipeline are from patients, a modification to the algorithm is employed to improve the segmentation of the bone surface. Instead of using the intensity values from the smoothed US image, intensity values from a phase filtered US image as described in Section 4.1.2 are used. An US slice is overlaid with the single pixel US bone surface using the original algorithm and the modified algorithm, respectively, in Figure 4.6. The phase modified algorithm picks up fewer bone surface pixels than the original algorithm. However, more importantly, less noise is seen in the modified algorithm. Having less noise is critical for an accurate

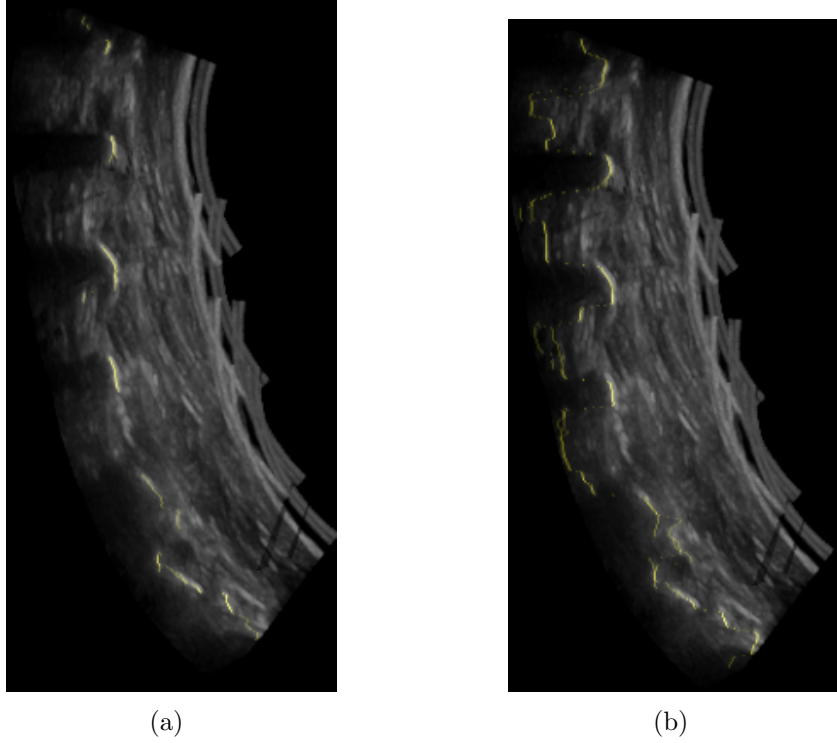


Figure 4.6: Sagittal US slice overlaid in yellow with the single pixel bone surface.
 (a) US slice using the modified algorithm; (b) US slice using the original algorithm.

point-based registration, since the presence of noise when limited bone surfaces are seen may drastically modify the registration result.

4.2.2 Point-based Global Rigid Registration

A point-based global rigid registration (step 2) is used following the intensity-based registration (step 1) to further improve the alignment achieved. The CPD algorithm developed by Myronenko *et al.* [40] used for the global rigid point-based registration uses probability density estimation to find corresponding points between the CT and US rather than finding the closest points between the two point sets as is done in the ICP and UKF-based approaches described in Section 2.3.1. One of the benefits for

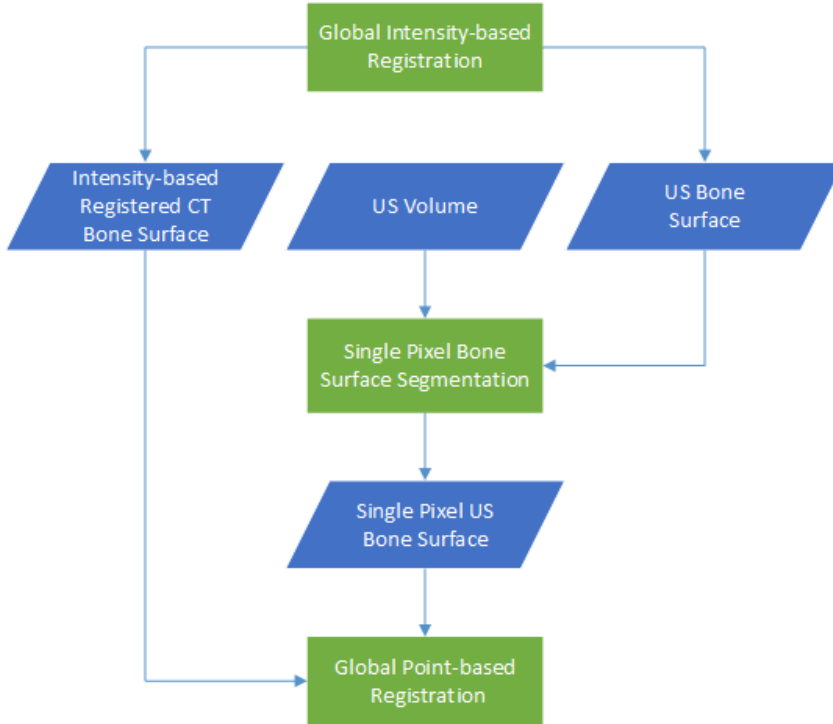


Figure 4.7: General overview of the point-based global rigid CPD registration. This figure is expanded from Figure 4.1.

this choice of point-based registration is that it has a closed-form solution in that it can be solved in a finite number of operations [40].

The moving point set is the CT bone surface from Section 4.1.1 and the fixed point set is the single pixel US bone surface from Section 4.2.1. An overview of step 2 is shown in Figure 4.7. Details on the CPD algorithm are explored next.

Rigid CPD Registration

The CPD algorithm aligns the CT and US point sets using probability density estimation [40]. The moving point set or the CT point set is modelled by a mixture of M Gaussian distributions, known as a GMM. This point set consists of vectors $\vec{y}_m, m = 1, 2, \dots, M$ and each vector represents a GMM centroid. The CT point set

used is derived from the bone surface described in Section 4.1.1. The fixed point set or the US point set is made up of vectors $\vec{x}_n, n = 1, 2, \dots, N$ and each vector corresponds to a data point that was generated from the GMM. The US point set was found using the single pixel bone surface detailed in Section 4.2.1. Both the vectors for the moving and fixed point set are D-dimensional, where $D = 3$. $T(\vec{y}_m, \theta)$ signifies a transformation T applied to the vectors \vec{y}_m , given a set of transformation parameters θ . The θ parameters consist of the three rotations in x, y, z , represented by a rotation matrix, and three translations along x, y, z . By applying the transformation T to all of the moving point set vectors \vec{y}_m , it is ensured that the GMM centroids move as a group to maintain the topology of the point set. To account for outliers, a uniform distribution is added to the GMM. The probability density function for a given vector \vec{x}_i is then expressed as:

$$p(\vec{x}) = \sum_{m=1}^{M+1} P(m)p(\vec{x}|m) \quad (4.3a)$$

$$= \omega(\text{UniformDistribution}) + (1 - \omega)(\text{GaussianDistribution}) \quad (4.3b)$$

$$= \omega \frac{1}{N} + (1 - \omega) \sum_{m=1}^{M+1} \frac{1}{M} G(\vec{x}|\vec{\mu}, \sigma^2), \quad (4.3c)$$

where ω corresponds to the weight given to the degree of outliers present, σ^2 represents the covariance, $\vec{\mu}$ is the mean. The gaussian distribution is further defined by:

$$G(\vec{x}|\vec{\mu}, \sigma^2) = (2\pi\sigma^2)^{-\frac{D}{2}} \exp\left(\frac{-\|\vec{x} - \vec{\mu}\|^2}{2\pi\sigma^2}\right) \quad (4.4)$$

In our case, $\vec{\mu}$ refers to $T(\vec{y}_m, \theta)$.

To measure the goodness of fit between the two point sets, the following objective function is used:

$$E = - \sum_{n=1}^N \log \sum_{m=1}^{M+1} P(m)p(\vec{x}_n|m) \quad (4.5)$$

When the objective function in equation(4.5) is maximized by adjusting the transformation parameters θ , the CT and US point sets are the most aligned according to the posterior probabilities calculated from the GMM. Formally, given two points \vec{x}_n and \vec{y}_m representing the data point and centroid respectively, the posterior probability is calculated as follows:

$$P(m|\vec{x}_n) = \frac{P(m)p(\vec{x}_n|m)}{p(\vec{x}_n)} \quad (4.6)$$

Maximizing the objective function in equation(4.5) is accomplished by maximizing the likelihood through the Expectation Maximization iterative algorithm [40]. The algorithm occurs in two steps: expectation and maximization. The expectation step consists of an initial guess for the parameters of the GMM, referred to as P_{old} . Initially the rotation matrix is the identity matrix and the translations in each x, y, z direction are each 0. The covariance σ_2 value is initially set to a larger value that should decrease at each iteration. The initial parameters are used to calculate the parameters to achieve new parameters P_{new} that ideally improve the alignment of the pointsets. P_{new} then become P_{old} and the process of the estimation and maximization steps are repeated.

The presented CPD algorithm by Myronenko *et al.* [40] uses point set correspondences through probability density estimation to improve the global intensity-based registration and to set up for the final step of the registration pipeline. The final step

involving multi-vertebrae point-based registration is expanded upon in the following section.

4.2.3 Multi-vertebrae Point-based Registration

The last major step in the registration pipeline, step 3, involves a multi-vertebrae point-based registration to account for possible curvature changes in the lumbar spine. Vertebrae are rigid bodies; however, the intervertebral discs are deformable. The rigid CPD algorithm is modified to define a novel multibody rigid CPD registration, where at each iteration, each vertebra is transformed individually. To maintain a relationship between the vertebra that are transformed individually, points are manually added preoperatively between each two adjacent vertebrae. Henceforward, these point sets are referred to as springs, since although they are not mechanical springs, they act to constrain the registration similarly to mechanical springs. The US point set based on the single pixel bone surface in Section 4.2.1 is the fixed point set for this step and is the same one that is used for the rigid point-based registration (Section 4.2.2). To apply a transformation to the individual vertebra in the CT, the CT point set needs to be labeled by the vertebra they represent. An expansion of this step is seen in Figure 4.8. The methodology for automatic labeling is outlined further in the subsections to follow. More details on the modifications to the original CPD algorithm [40] to develop the novel multibody CPD algorithm are also presented.

Labeling CT Points

The CT bone surface transformed by the global intensity-based registration (step 1) then the global point-based registration (step 2) is the input to the multibody CPD

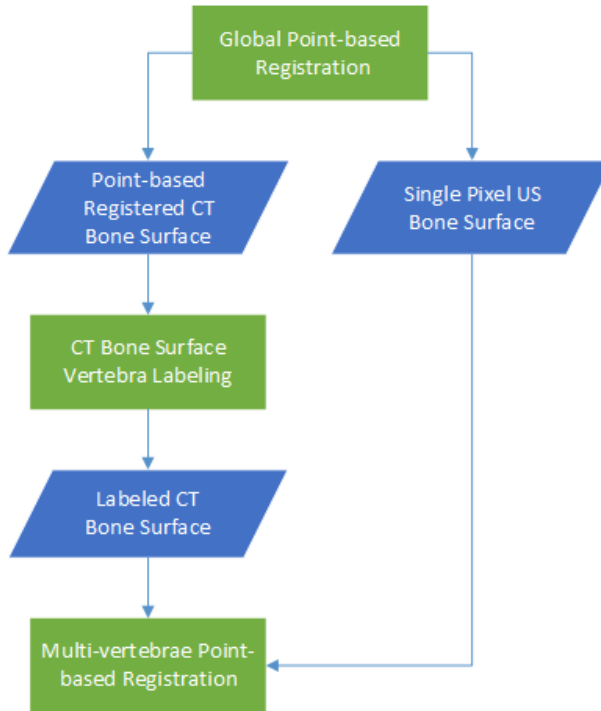


Figure 4.8: General overview of the multi-vertebrae point-based registration. This figure is expanded from Figure 4.1.

registration. Obtaining this bone surface was described in Section 4.1.1. An additional step that is needed in order to consider the vertebrae as multiple rigid bodies is vertebral labeling of the points in the CT.

A Python script was developed and used in the Python console within the 3D Slicer [46] [47] environment to automatically label the points in the bone surface based on the vertebra they belong to. The labels used in the developed code are extracted from an automatic segmentation algorithm developed by Rasoulian *et al.* [52]. The automatic segmentation is performed by a surface to surface registration of a multi-vertebrae statistical shape and pose model to the CT. This approach uses an iterative Expectation Maximization algorithm similar to the one described in Section 4.2.2 to align the statistical shape and pose model to the outline of the CT found through

Canny edge detection of the transverse slices.

Rigid Multibody CPD Registration

The rigid CPD algorithm was discussed previously in Section 4.2.2 and is used as the rigid component for the multi-vertebrae point-based registration. In Section 4.2.2, all the points in the CT point set representing multiple vertebrae are used to register the CT point set to the US point set. Here, modifications to the rigid CPD algorithm are done in order to find a rigid transformation for each vertebra during each iteration. This means that there are six parameters for each vertebra consisting of three rotations in x, y, z and three translations along x, y, z . Creating point sets for each vertebra is done through the labeling described in Section 4.2.3. The US point set is unaltered from the rigid CPD registration in Section 4.2.2 and is also used as the fixed point set for this step.

Since the vertebrae are transformed individually at each iteration in the multi-vertebrae point-based registration, it is possible that they can be transformed into a pose of the lumbar spine that is not physically possible. To overcome this challenge, ten points are preoperatively chosen manually between two adjacent vertebra. Five points on the sagittal slices on the left of the spinous process and five points on the right of the spinous process. An example sagittal slice where three points are chosen is shown in Figure 4.9. No more than three points are selected on one slice to make sure the springs are evenly spread throughout the CT volume. The points are placed at the midpoint of either the space between the vertebral bodies or the space between the facet joint. Each point is then duplicated to act as a spring, where one point belongs to the superior vertebrae's side and the other point belongs to the inferior

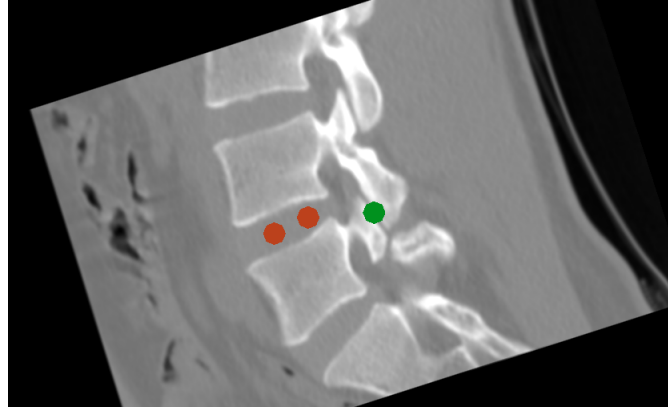


Figure 4.9: Sagittal slice of a CT demonstrating three spring points that were manually chosen between two adjacent vertebrae. Two are approximately at the midpoint in the space between two adjacent vertebral bodies (shown in red). One point is within the facet joint (shown in green).

vertebrae's side. At each iteration, the springs points are transformed based on the vertebrae they belong to. When the registration first begins, the distance between the two points that represent a spring is zero, since they are a duplication of the point.

To incorporate the springs in the multi-vertebrae point-based registration, a value α is used to weight the effect of the springs. The objective function did not need to be modified as the springs are added to the existing matrix P representing how likely a point in the CT point set corresponded to a point in the US point set. The additions to P involving the springs have probabilities of zero for the correspondences between the CT point set and US point set, since the spring point set is unrelated and does not share any correspondence with the US data set.

A simplified example is presented to demonstrate how the springs are incorporated into the matrix P . Given: one spring between the L3 and L4 vertebrae, three CT points in the CT point set represented as CT_1 , CT_2 , CT_3 , respectively and three US points in the US point set represented as US_1 , US_2 , US_3 , respectively, matrix P is

represented as:

$$P = \begin{bmatrix} P(CT1|US1) & P(CT2|US1) & P(CT3|US1) & 0 \\ P(CT1|US2) & P(CT2|US2) & P(CT3|US2) & 0 \\ P(CT1|US3) & P(CT2|US3) & P(CT3|US3) & 0 \\ 0 & 0 & 0 & \alpha \end{bmatrix}$$

$P(CT1|US1)$ represents how likely point $CT1$ corresponds to $US1$. The spring point between the L3 and L4 vertebrae has one side on the L3 vertebra and one side on the L4 vertebra. The spring point on the L3 vertebra will be referred to as $springL3$ and the spring point on L4 will be referred to as $springL4$. $springL3$ is appended to the US point set matrix ($USPoints$) and the $springL4$ is appended to the CT point set matrix ($CTPoints$) as follows:

$$USPoints = \begin{bmatrix} US1_x & US1_y & US1_z \\ US2_x & US2_y & US2_z \\ US3_x & US3_y & US3_z \\ springL3_x & springL3_y & springL3_z \end{bmatrix}$$

$$CTPoints = \begin{bmatrix} CT1_x & CT1_y & CT1_z \\ CT2_x & CT2_y & CT2_z \\ CT3_x & CT3_y & CT3_z \\ springL4_x & springL4_y & springL4_z \end{bmatrix}$$

Each row is a point in the point set and each column corresponds to the x, y, z point coordinates, respectively. The simplified example shows that the springs are integrated into the existing matrices used in the probability density estimation.

α value of 2^5 was used for all cases. A value of α between 2^{-3} to 2^7 was tested and a value of 2^5 provided the most accurate registration for all five clinical data sets. The novel multi-vertebrae point-based registration represented the final step of the registration pipeline.

4.3 Summary

This chapter described the automatic registration pipeline that was used to align the clinical CT volume to the US volume. The three major steps of the pipeline, including global intensity-based registration, global point-based registration and multi-vertebrae point-based registration were presented in detail. The work involved bridging many existing algorithms from different contexts into a pipeline that would align the clinical lumbar spine data. Modifications to certain algorithms were needed to apply the algorithms for a lumbar spine CT to US registration. The existing single pixel bone surface algorithm [17] used for the point-based registration was modified to output a less noisy single pixel bone surface of the clinical US. The CPD algorithm [40] was altered to create a novel multi-vertebrae point-based registration to account for the change in curvature between the vertebrae. Together, the existing algorithms and critical modifications make up a robust registration pipeline. The next chapter presents the results obtained using the registration workflow presented here. Results given modifications to the pipeline are also shown to demonstrate the need for various steps in the workflow.

Chapter 5

Results and Discussion

In this chapter, the results generated by the automatic registration pipeline presented in the previous chapter are shown and discussed. The registration workflow is validated on five patient data sets. The quantitative validation approach was previously described in detail in Section 3.3.

Qualitative results are discussed for each of the five patients. Images showing the outlines of the CT overlaid on the US volume are shown in the transverse, sagittal and coronal planes along with a 3D rendering of the CT. Visualizations are all done in 3D Slicer [46] [47] (Section 2.4.3). As previously mentioned in Section 3.3, points placed on the posterior dura in the US will provide a qualitative validation showing whether a needle would be guided to the correct space using the aligned CT for spinal anesthesia. These points are shown in 3D with the 3D rendering of the CT.

For quantitative results, capture range experiments are presented for all five patient data sets. Details of these capture range experiments were described in Section 3.3 and involve perturbing the CT that is aligned to the US by 20 random initial transformations. The initial transformations are selected from a uniform distribution for 5° rotation about each axis and 5 mm translation along each axis. Results for the

following five capture range experiments are outlined to demonstrate the need for the different components of the registration workflow to enable robust registration:

1. Registration pipeline described in Chapter 4.
2. Registration pipeline without the global intensity-based registration (Section 4.1), referred to as step 1 of the registration workflow.
3. Registration pipeline given the unmodified single pixel US bone surface (Section 4.2.1) as input to the point-based registrations.
4. Registration pipeline without the global point-based registration (Section 4.2.2) referred to as step 2 in the registration workflow.
5. Registration pipeline without the use of the springs in the multi-vertebrae point-based registration (Section 4.2.3).

Table 5.1 describes the lumbar vertebrae included in the registration for each patient. All the patient CT images included only a portion of the lumbar spine.

Table 5.1: Lumbar vertebrae in the CT that are registered for each of the five patients.

Dataset	Lumbar Vertebrae
Patient 1	L3, L4, L5
Patient 2	L3, L4, L5
Patient 3	L3, L4, L5
Patient 4	L4, L5
Patient 5	L4, L5

Table 5.2: Runtime range in seconds for each of the registration components in the pipeline.

Registration Step	Runtime Range (seconds)
Intensity-based (step 1)	5–20
Point-based (step 2)	25–45
Multi-vertebrae (step 3)	20–120

5.1 CT to US Registration Results using the Proposed Pipeline

This section shows the results attained from running the registration pipeline presented in Chapter 4 on five patient datasets. The runtime for each of the main registration components of the pipeline are shown in Table 5.2. The registration pipeline was performed on a Lenovo ThinkCenter, with Intel i5-3570 quad-core CPU and 16 GB of RAM.

For capture range experiments, an average of 94% success rate is achieved. Rasoulian *et al.* [50] defines 2 to 4 mm as a clinically acceptable accuracy for epidural injections. The space within a facet joint is reported to be between 2 to 4 mm [51]. Success is then defined as achieving a mean TRE of 2 mm or less to provide a conservative estimate of clinical acceptability. The final TRE after each run of the capture range experiment given the initial misalignment TRE for all five patients is shown in Figure 5.1. All reported TRE values are the average of the TRE for each individual vertebra registered. The mean TRE is the average of the TRE values from the 20 runs of the capture experiments. The mean TRE, maximum point distance and total success rate for each patient is depicted in Table 5.3. From the results in the table, it is evident that the mean TRE fits well below 2 mm.

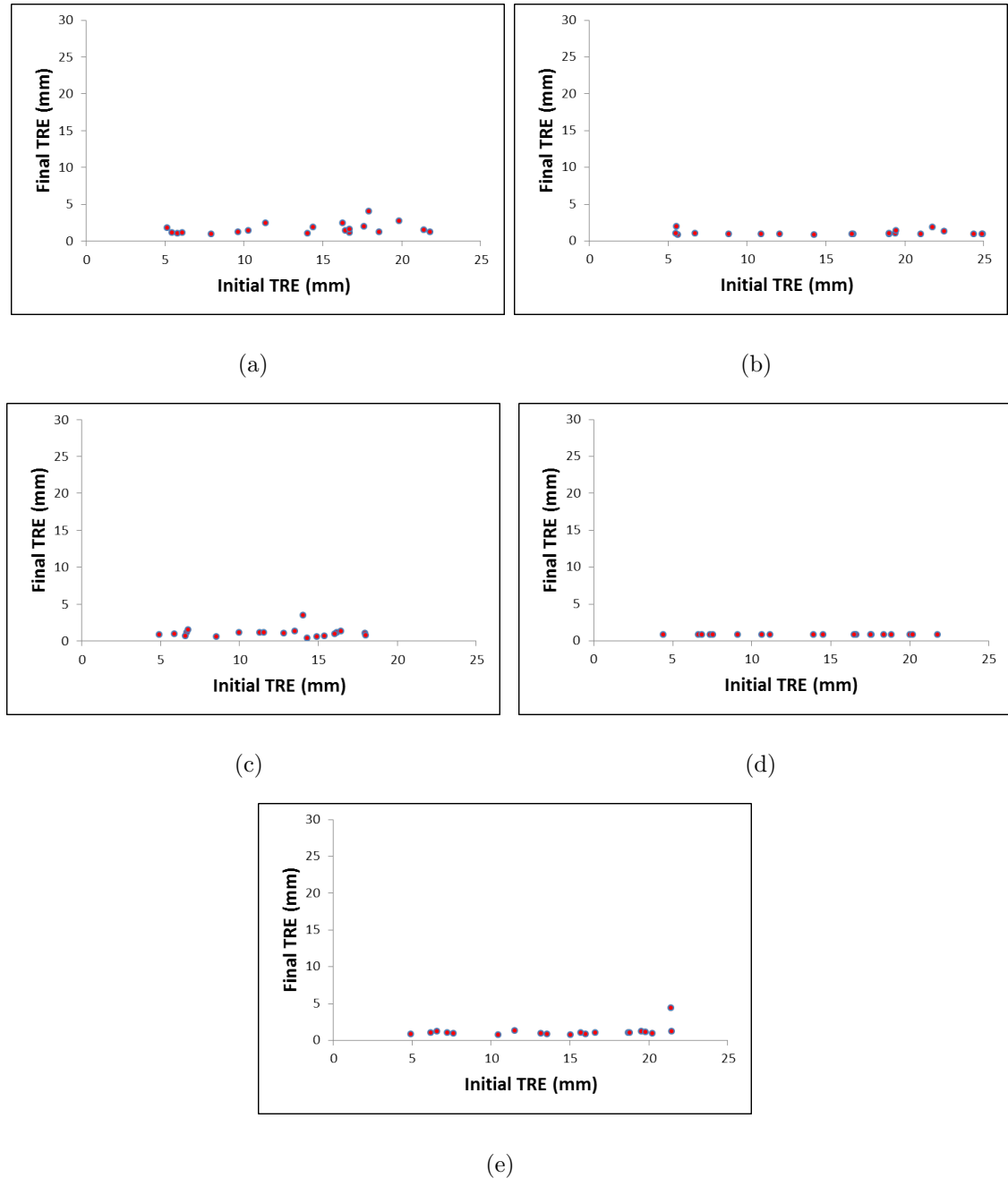


Figure 5.1: Plot of the final mean TRE (mm) for all vertebrae between the CT and US data after the registration pipeline given the initial TRE (mm) after the random initial misalignment. (a) patient 1; (b) patient 2; (c) patient 3; (d) patient 4; (e) patient 5.

Table 5.3: Mean TRE (mm), maximum point distance (mm) and total success rate from the CT to US registration for the five patients using the full registration pipeline.

dataset	mean TRE \pm std (mm)	maximum point distance (mm)	total success rate
Patient 1	1.66 \pm 0.77	4.61	16/20
Patient 2	1.09 \pm 0.32	3.51	20/20
Patient 3	1.07 \pm 0.64	3.76	19/20
Patient 4	0.85 \pm 0.01	0.90	20/20
Patient 5	1.18 \pm 0.77	4.64	19/20

To provide a qualitative validation, contours of the CT are overlaid on the sagittal, transverse and coronal planes of the US illustrated in Figure 5.2 for patient 1, Figure 5.3 for patient 2, Figure 5.4 for patient 3, Figure 5.5 for patient 4 and Figure 5.6 for patient 5. There is also a 3D rendering of the CT with a point on the posterior dura between each two adjacent vertebrae representing the target area for spinal anaesthesia. This provides a clinically relevant result to support the quantitative validation. The posterior dura points are placed on the US images by two operators to clinically validate the CT alignment after registration. From Figures 5.2, 5.3, 5.4, 5.5 and 5.6, the CT contours align in all three planes and the points on the posterior dura are all within the target area for spinal anesthesia. Points placed on the posterior dura between adjacent vertebrae may be on different US slices and therefore, all of the points may not be visible in the coronal slice shown.

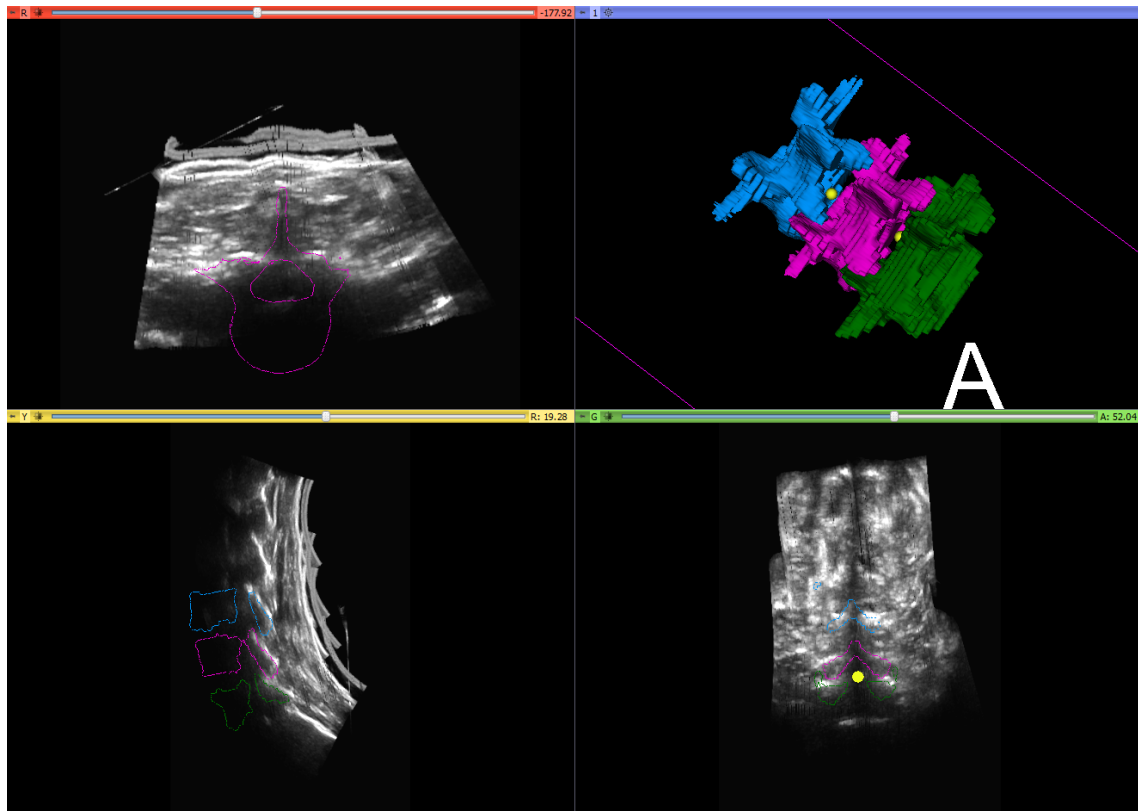


Figure 5.2: 3D rendering of CT vertebrae with points on the posterior dura between two vertebrae (represented in yellow) on the top right and sagittal (bottom left), transverse (top left) and coronal (bottom right) planes showing US slices with the CT contours overlaid for patient 1.

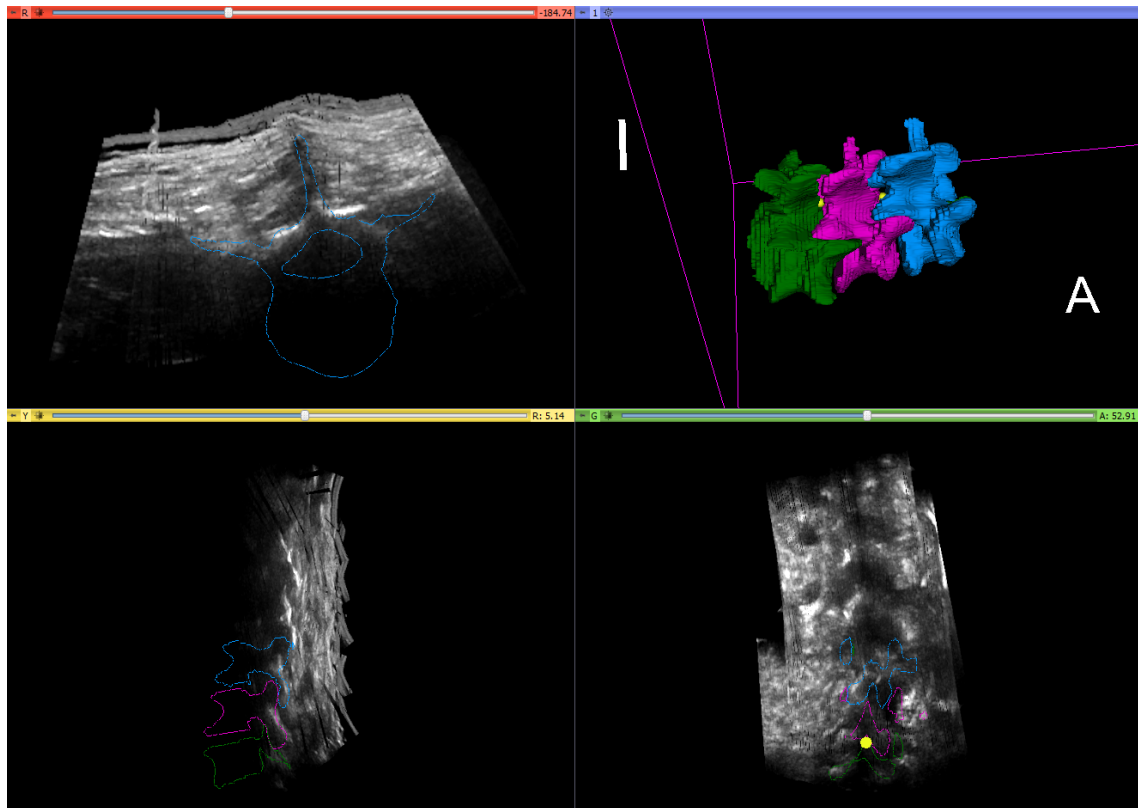


Figure 5.3: 3D rendering of CT vertebrae with points on the posterior dura between two vertebrae (represented in yellow) on the top right and sagittal (bottom left), transverse (top left) and coronal (bottom right) planes showing US slices with the CT contours overlaid for patient 2.

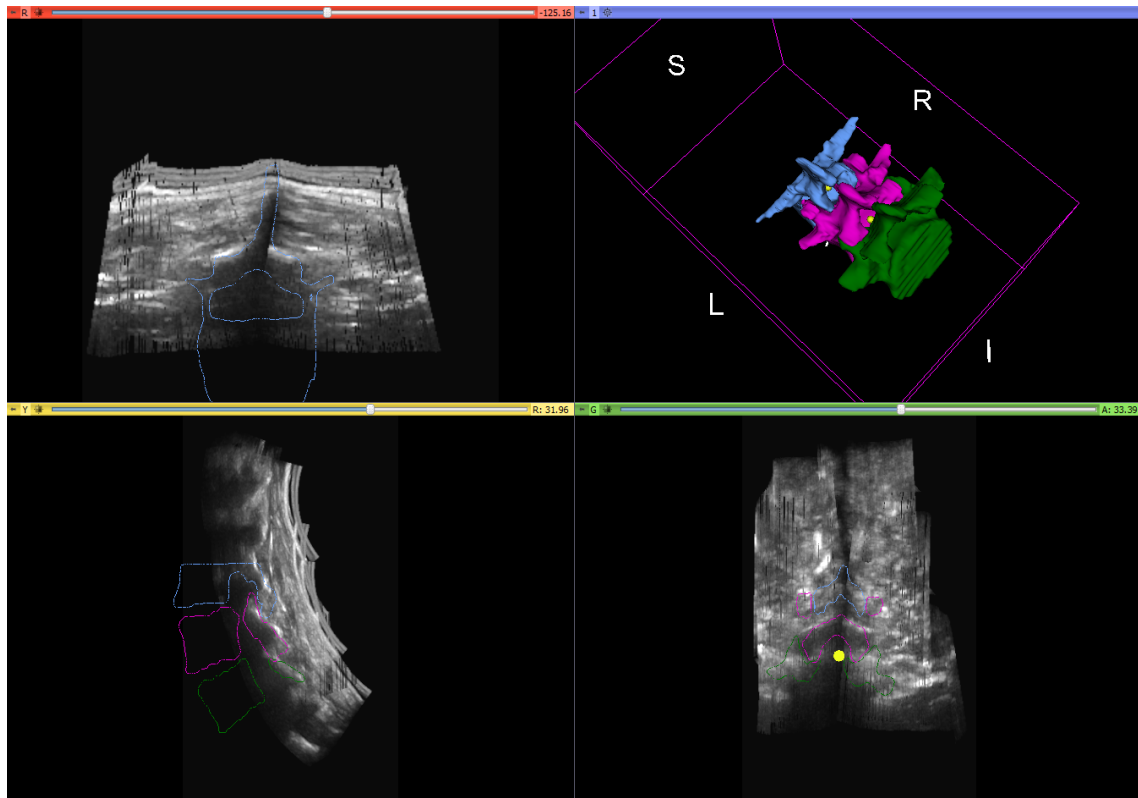


Figure 5.4: 3D rendering of CT vertebrae with points on the posterior dura between two vertebrae (represented in yellow) on the top right and sagittal (bottom left), transverse (top left) and coronal (bottom right) planes showing US slices with the CT contours overlaid for patient 3.

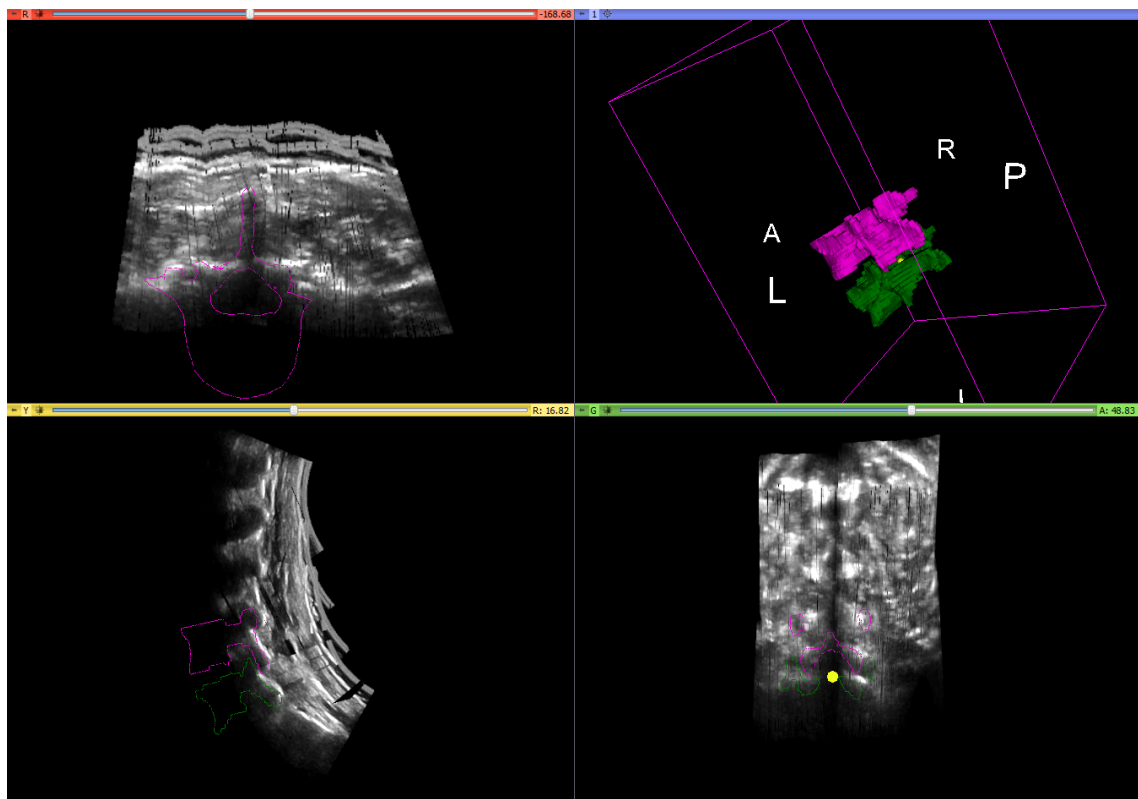


Figure 5.5: 3D rendering of CT vertebrae with points on the posterior dura between two vertebrae (represented in yellow) on the top right and sagittal (bottom left), transverse (top left) and coronal (bottom right) planes showing US slices with the CT contours overlaid for patient 4.

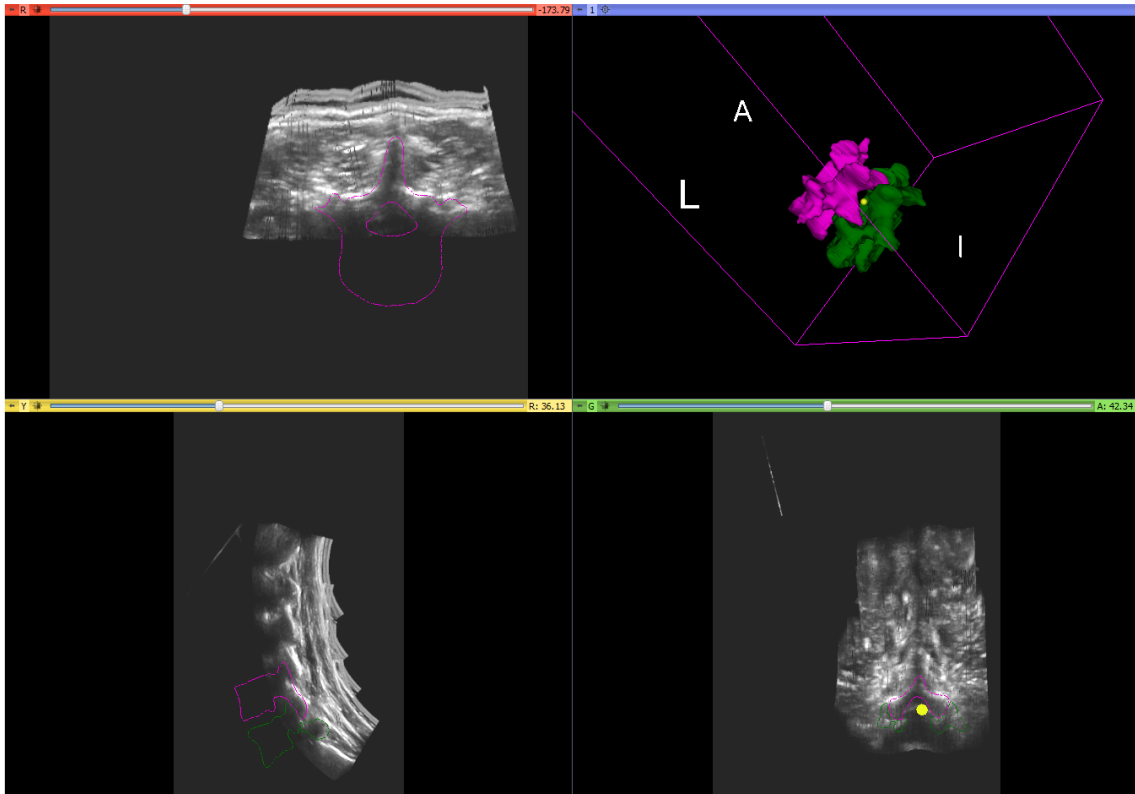


Figure 5.6: 3D rendering of CT vertebrae with points on the posterior dura between two vertebrae (represented in yellow) on the top right and sagittal (bottom left), transverse (top left) and coronal (bottom right) planes showing US slices with the CT contours overlaid for patient 5.

Since the registration pipeline is extensive in that it involves global intensity-based, global point-based and multi-vertebrae point-based registration, several capture range results are generated to demonstrate the effect of all the components in the pipeline. Modifications are made to the algorithm by Foroughi *et al.* [17] to attain a less noisy single US bone surface (Section 4.2.1). In addition to verify the effect of removing steps from the pipeline, the result of modifying this existing algorithm is also examined. Using the existing algorithm by Foroughi *et al.* [17] will be referred to as the

unmodified single pixel US bone surface. To determine if there is a significant difference in the TRE using the proposed pipeline compared to a modified version, p-values are calculated using the Wilcoxon Signed-Rank Test, where $p < 0.01$ is considered significant.

5.1.1 The Effect of the Intensity-based Registration Step

CT to US registration results are evaluated without the global intensity-based registration (step 1). The global intensity-based registration involves aligning the bone surfaces in the CT and US that are automatically enhanced using local phase filtering (Section 4.1). The results of the capture range experiments when the global intensity-based registration is not included in the registration pipeline for all five patients are shown in Figure 5.7. From the capture range experiments, patient 1, patient 4 and patient 5 did not show a significant difference in the TRE without the intensity-based registration ($p = 0.02$, $p = 0.03$, $p = 0.39$ respectively). Patient 2 and patient 3 did show a significant difference with an increased TRE ($p < 0.001$, $p < 0.001$, respectively). Removing the intensity information and using solely point information is problematic for patient 2 and patient 3 as there is limited US bone visibility in these datasets. Table 5.4 shows that only patient 4 and patient 5 have a mean TRE less than 2 mm. Patient 1's mean TRE is negatively affected by three runs of the capture range experiment. These three misalignments have a large rotation about both the z and y axes that the pipeline could not correct without intensity information. It is therefore more robust to include the global intensity-based registration as the first step to provide a rough registration between the CT and US.

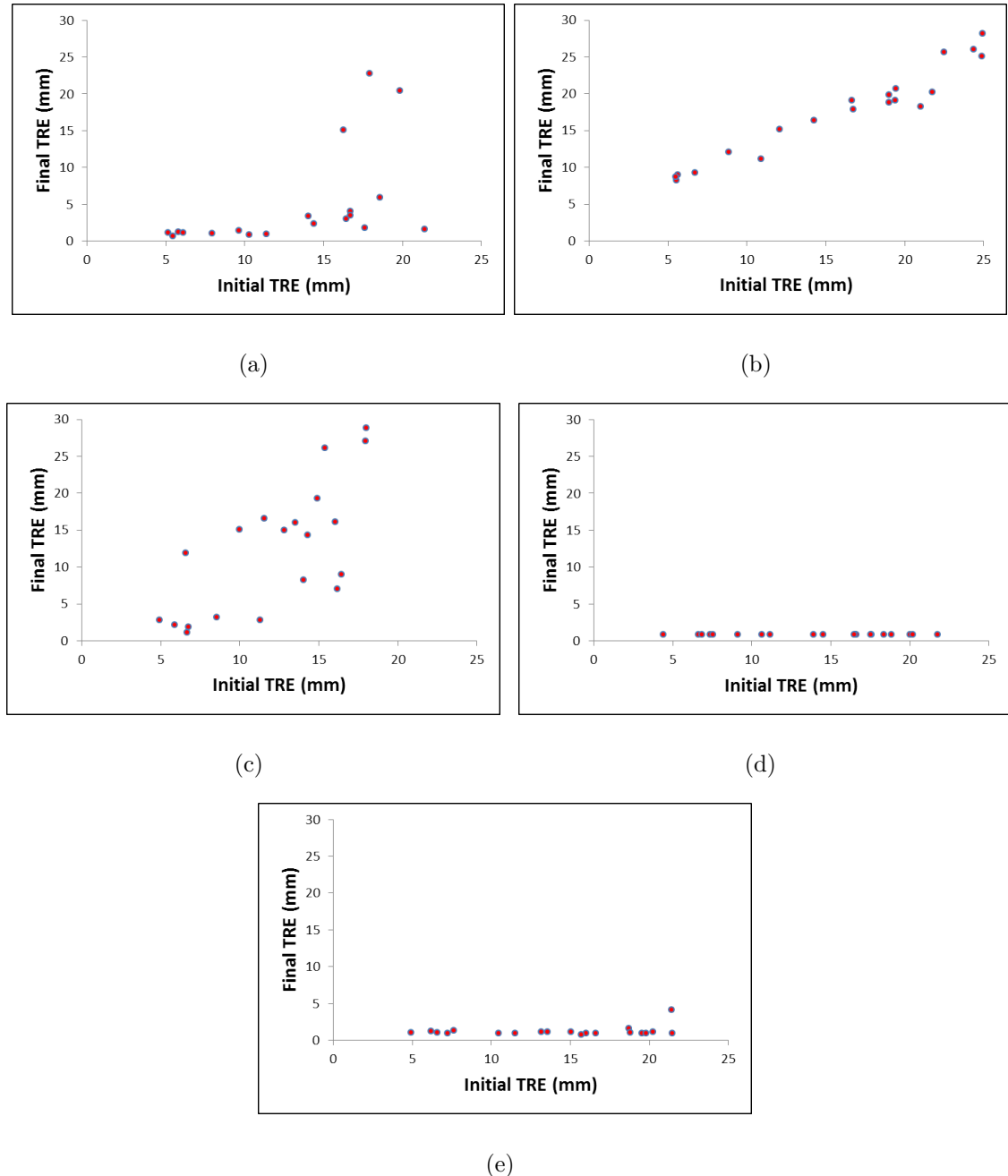


Figure 5.7: Plot of the final TRE (mm) between the CT and US data after the modified registration pipeline given the initial TRE (mm) following the random initial misalignment. The pipeline was modified to eliminate the intensity-based registration step. (a) patient 1; (b) patient 2; (c) patient 3; (d) patient 4; (e) patient 5.

Table 5.4: Mean TRE (mm) and maximum point distance (mm) from the CT to US registration for the five patients using a modified registration pipeline, where the intensity-based registration step is not performed.

Dataset	mean TRE \pm std (mm)	maximum point distance (mm)
Patient 1	6.16 \pm 8.85	39.3
Patient 2	18.38 \pm 5.79	30.4
Patient 3	12.2 \pm 8.75	29.8
Patient 4	0.84 \pm 0.01	0.91
Patient 5	1.19 \pm 0.77	4.63

5.1.2 The Effect of using the Unmodified Single Pixel US Bone Surface

Next, using the unmodified single pixel US bone surface for the point-based registrations is examined to see if the modifications to reduce noise are needed. Details on the modifications to the algorithm were discussed in Section 4.2.1. The results of the capture range experiments using the unmodified single pixel US bone surface as input for the point-based registrations are shown in Figure 5.8. Patient 1, patient 4 and patient 5 have a significant loss in accuracy ($p = 0.007$, $p < 0.001$, $p = 0.001$, respectively) relative to the full registration pipeline. Patient 2 and patient 3 have a success rate of 0/20 and show a significant increase in the TRE ($p < 0.001$, $p < 0.001$, respectively). From Table 5.5, only the mean TRE for patient 5 is within the acceptable 2 mm range. In all cases, the original algorithm contains more noise relative to the modified algorithm. As mentioned previously, patient 2 and patient 3 have a limited number of points that represent the bone surface. Therefore, having more noise skews the registration and results in an inaccurate registration.

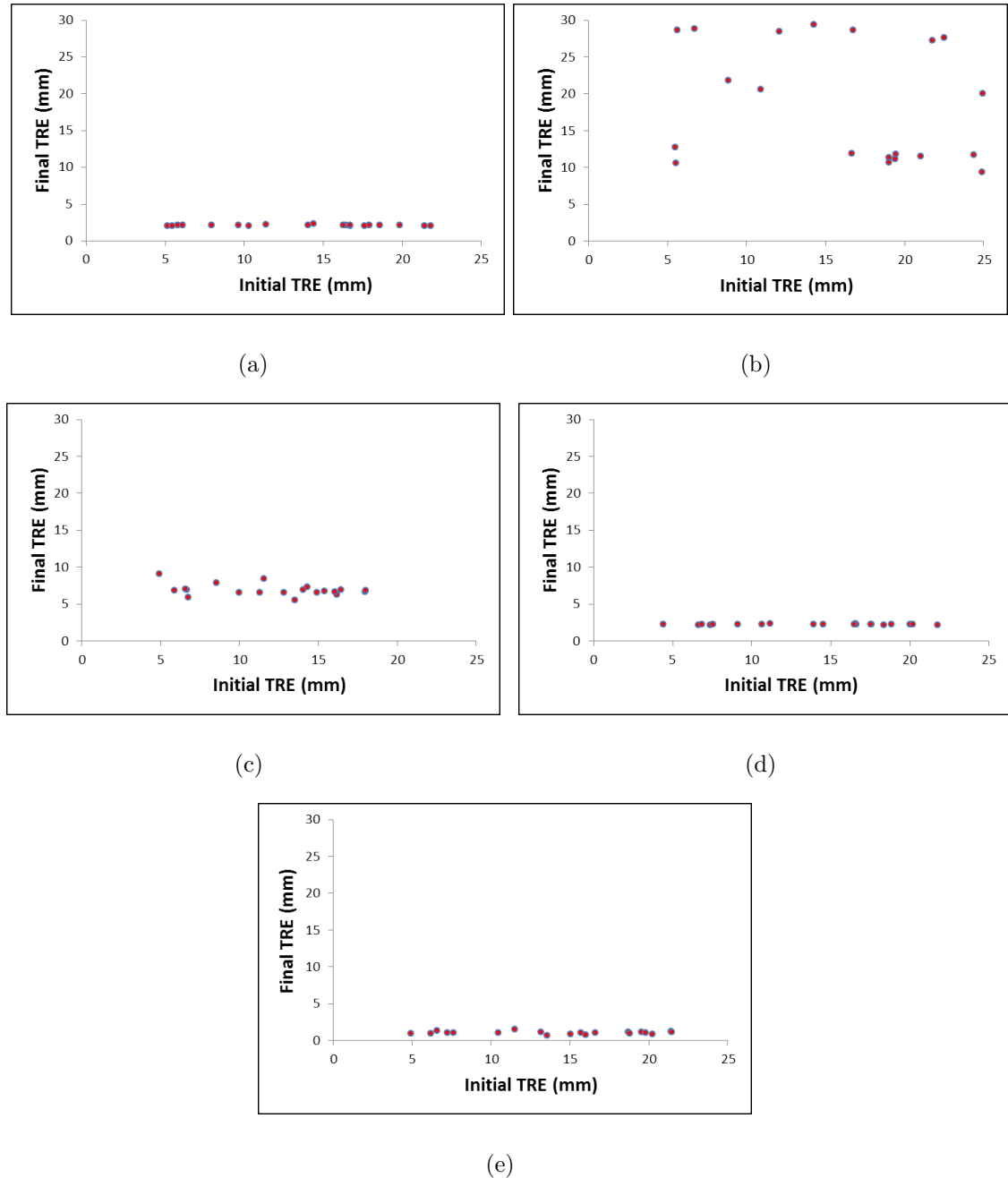


Figure 5.8: Plot of the final TRE (mm) between the CT and US data after the modified registration pipeline versus initial TRE (mm) following the random initial misalignment. The pipeline was modified to use the unmodified single pixel US bone surface.(a) patient 1; (b) patient 2;(c) patient 3; (d) patient 4; (e) patient 5.

Table 5.5: Mean TRE (mm) and maximum point distance (mm) from the CT to US registration for the five patients using a modified registration pipeline, where the unmodified single pixel US bone surface was used.

Dataset	mean TRE \pm std (mm)	maximum point distance (mm)
Patient 1	2.13 ± 0.07	3.20
Patient 2	17.6 ± 7.72	31.91
Patient 3	6.90 ± 0.80	9.83
Patient 4	2.23 ± 0.05	3.04
Patient 5	1.01 ± 0.18	1.54

5.1.3 The Effect of the Global Point-based Registration Step

Since a global intensity-based registration is part of the registration pipeline to attain a rough estimate of the alignment between the CT and US, determining whether the global point-based registration is necessary is considered next. The results of the capture range experiments when the global point-based registration is not included in the registration pipeline for all five patients are shown in Figure 5.9. There is a significant increase in the TRE for patient 1, patient 2, patient 3 and patient 5 ($p < 0.001$, $p < 0.001$, $p < 0.001$, $p < 0.001$, respectively). Patient 4 did not show a significant difference in the accuracy ($p = 0.052$). Table 5.6 shows that the mean TRE for all patients are too high for clinical use in percutaneous spinal interventions. Patient 4 had 6/20 runs that were unsuccessful and negatively affected the mean TRE. In these cases, the intensity-based registration incorrectly aligned the CT vertebral bodies to the lamina of the US. The global point-based registration corrects instances where the global intensity-based registration does not provide a close initial alignment

between the CT and US. Since the final registration step is constrained by the springs, movement occurs between adjacent vertebrae. A close global alignment is required as there is limited global movement of all vertebrae in the multi-vertebrae registration.

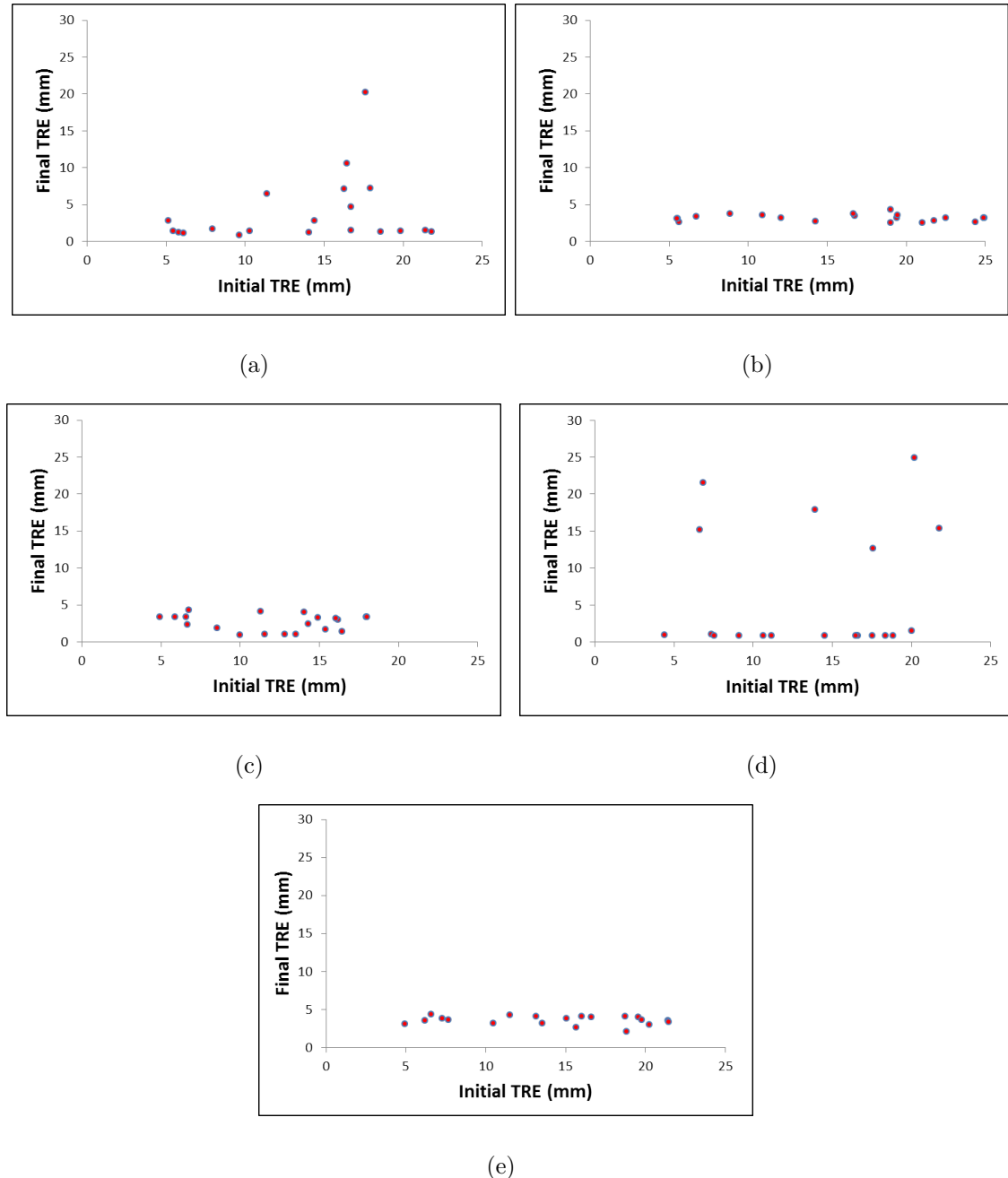


Figure 5.9: Plot of the final TRE (mm) between the CT and US data after the modified registration pipeline given the initial TRE (mm) following the random initial misalignment. The pipeline was modified to eliminate the global point-based registration step. (a) patient 1; (b) patient 2; (c) patient 3; (d) patient 4; (e) patient 5.

Table 5.6: Mean TRE (mm) and maximum point distance (mm) from the CT to US registration for the 5 patients using a modified registration pipeline, where the global point-based registration step is not performed.

Dataset	mean TRE \pm std (mm)	maximum point distance (mm)
Patient 1	3.89 ± 4.72	23.0
Patient 2	3.21 ± 0.47	5.45
Patient 3	2.62 ± 1.14	5.05
Patient 4	6.01 ± 8.34	27.4
Patient 5	3.56 ± 0.59	3.90

5.1.4 The Effect of Springs in the Piecewise Point-based Registration Step

In the last stage of the registration pipeline, springs are used to constrain the multi-vertebrae point-based registration. More details on the springs were provided in Section 4.2.3. As vertebrae are the rigid bodies transformed individually at each iteration of the registration, registration can result in a pose of the lumbar spine that is not physically possible. This includes having two vertebrae intersect each other (collision). The results of the capture range experiments when the springs have no effect (given an α value of 0) on the multi-vertebrae point-based registration for all five patients are shown in Figure 5.10. Patient 1, patient 4 and patient 5 have a significant loss in accuracy ($p < 0.001$, $p < 0.001$, $p = 0.001$, respectively) compared to when the full registration workflow is employed. In these cases, either the vertebrae move too close or too far relative to each other in the absence of the springs. The mean TRE values are reported for patient 2 and patient 3, however both of these alignments

were not a physically possible pose of the lumbar spine. Therefore, the TRE values may be meaningless. Patient 2 has 0/20 successful runs as all three vertebrae moved into a pose of the spine that was not physically possible and resulted in a significant increase in the TRE ($p < 0.001$). An example of this is shown in Figure 5.11. Patient 3 also has 0/20 successful runs. The L3 vertebra caused a significant increase in the TRE ($p < 0.001$) as it collided with the L4 vertebra in all runs. There is limited bone visibility for L3 and when its movement is not constrained by the springs, the vertebra was matched to US bone surface points belonging to L4. Only patient 4 has a clinically acceptable mean TRE value.

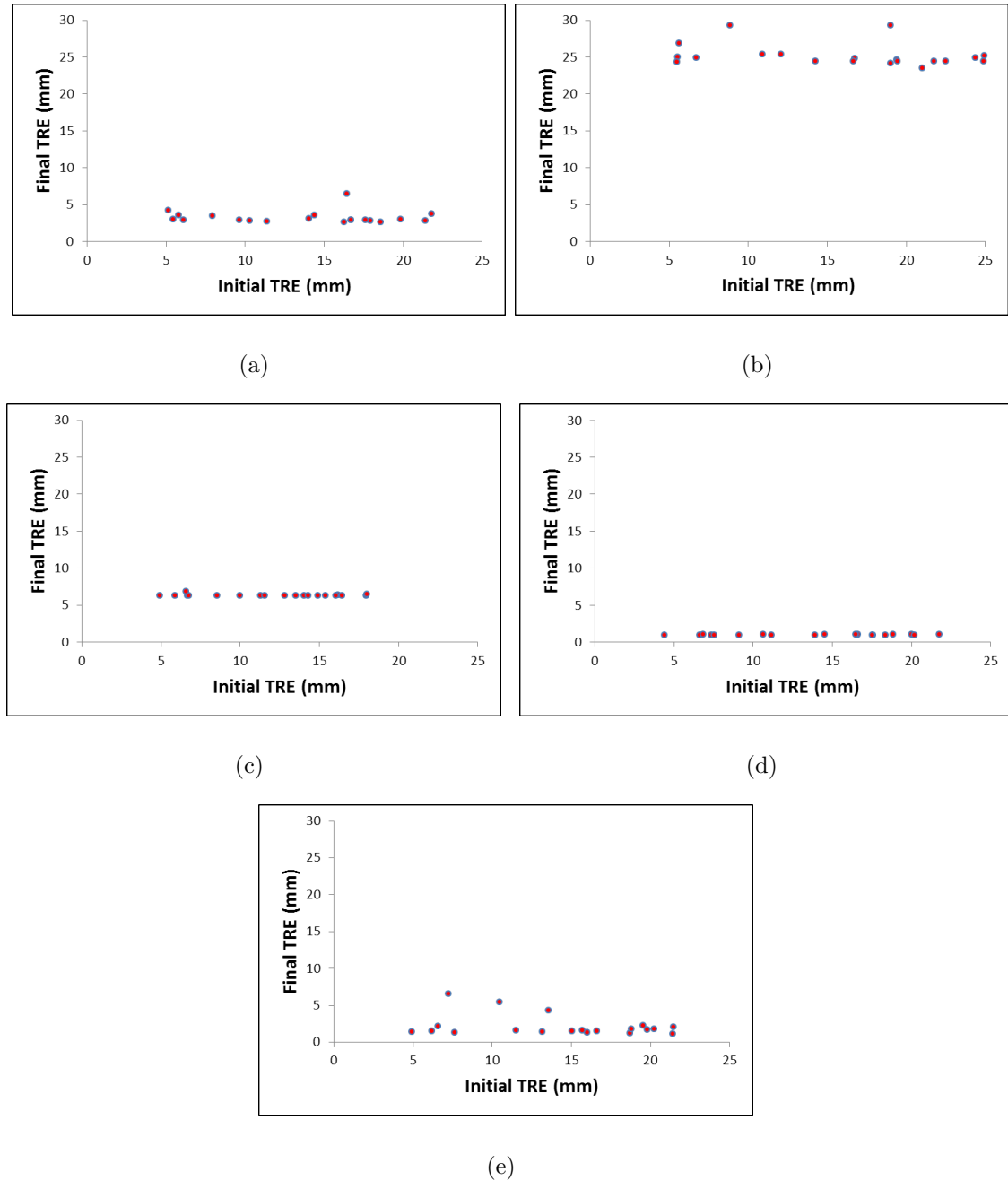


Figure 5.10: Plot of the final TRE (mm) between the CT and US data after the modified registration pipeline given the initial TRE (mm) following the random initial misalignment. The pipeline was modified to remove the springs in the piecewise point-based registration. (a) patient 1; (b) patient 2; (c) patient 3; (d) patient 4; (e) patient 5.

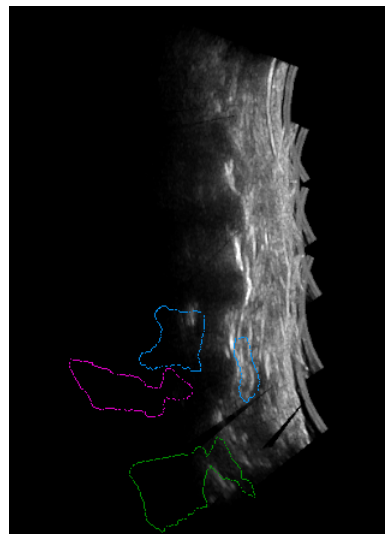


Figure 5.11: Registration result after one run for patient 2 showing that the lumbar spine pose is not physically possible.

Table 5.7: Mean TRE (mm) and maximum point distance (mm) from the CT to US registration for the five patients using a modified registration pipeline, where the springs in the piecewise point-based registration are not used.

Dataset	mean TRE \pm std (mm)	maximum point distance (mm)
Patient 1	3.26 ± 0.86	14.99
Patient 2	25.1 ± 1.58	45.99
Patient 3	6.33 ± 0.14	8.96
Patient 4	0.98 ± 0.01	1.20
Patient 5	2.17 ± 1.48	7.06

5.2 Summary

This chapter demonstrated that the registration pipeline developed to align clinical CT data to US data for percutaneous spine needle injections is clinically feasible. All

patient data were registered with a mean TRE below 2 mm. A qualitative validation showing a target point in the region for spinal anaesthesia demonstrated that the alignment achieved for all patients was clinically usable. To verify that all components of the pipeline were needed, four additional capture range experiments were conducted. By removing or modifying steps in the pipeline, not all patients had alignments that were clinically acceptable without the components of the registration. Therefore, to provide the most robust registration that covers the variability in quality in the US data of patients, the presented registration pipeline should be employed.

Chapter 6

Conclusions and Future Work

In this chapter, the contributions and findings in this thesis are summarized and suggestions for future directions of this research are outlined.

6.1 Summary of Conclusions

A registration pipeline for the lumbar spine was developed that accurately aligns preoperative CT to intraoperative US using five clinical datasets. By aligning the CT with the US, anatomical information that is not visible in US is provided to the clinician without having to expose the physician or patient to more radiation intraoperatively. There are many benefits of US, such as its real-time imaging, portability and low cost. These can now be used for percutaneous spine needle navigation, since the difficulties in interpretation can be overcome through the integration of anatomical information in CT images.

The registration pipeline in this thesis was designed with the following features in mind to help achieve a clinically acceptable method:

1. Variability in the image quality of US used as the fixed image in the registration

was decreased through an US data collection protocol. Parameters to automatically enhance the bone surface from the US for registration did not need to change between patients as their image quality was similar.

2. Preoperatively, springs were incorporated in the CT. Intraoperatively, a novel automatic multi-vertebrae point-based registration was developed, where each vertebra was individually registered to account for a possible curvature change between the preoperative CT taken in the supine position and the intraoperative US taken in the prone position. The springs acted to constrain the registration to output a pose of the lumbar spine that is physically possible.
3. The acoustic shadowing of the spine and noise inherent to US greatly affect CT to US registration. Local phase filtering overcame this by enhancing the US bone surface used in the registration pipeline.

The registration pipeline was validated on five clinical datasets. Capture range experiments were run and consisted of perturbing the registered CT by 20 random initial transformations selected from a uniform distribution for 5° rotation about each axis and 5 mm translation along each axis. Then, registration began with an initial misalignment of up to 25 mm. The capture range experiments demonstrated that all steps in the registration pipeline are needed for an accurate and robust registration. The outcome of each capture range experiment is summarized as follows:

1. The proposed registration pipeline: a mean TRE of 1.17 mm was achieved, which is clinically acceptable.
2. Removing the global intensity-based registration step: when limited points from the bone surface are available in the US point set, the global intensity-based

registration proved to be vital to the success of the alignment.

3. Removing the global point-based registration: In cases where the global intensity-based registration did not provide a close enough alignment for the multi-vertebrae point-based registration, a global point-based registration was needed.
4. Modifying the algorithm to extract the single pixel US bone surface: the modified algorithm reduced the noise in the US bone surface and improved the registration accuracy.
5. Removing the springs: without the springs in the multi-vertebrae registration, vertebrae in the lumbar spine collided in some cases, which is an unacceptable pose of the lumbar spine.

These results demonstrate that the proposed registration pipeline is accurate and robust using clinical data. There are however clinical requirements that should be improved to incorporate this registration pipeline into a clinical setting for percutaneous needle interventions.

6.2 Future Work

The proposed registration pipeline shows great promise for guiding percutaneous spine needle procedures, but further improvements are needed for its clinical use. The following improvements are suggested:

1. Evaluate the efficacy of the pillow beneath the patient's stomach during US data acquisition to determine if it affects CT to US registration.

2. Create a registration module for the pipeline in the open-source software 3D Slicer. 3D Slicer is a good platform for the user interface of the registration because visualization and analysis are built-in. Recently, a MatlabBridge extension was incorporated into 3D Slicer where Matlab functions can run directly in 3D Slicer. Since a lot of the preprocessing and registrations are run in Matlab, the MatlabBridge extension will be very useful.
3. The registration is automatic except for the selection of the artificial spring points that are manually chosen. Although this can be done preoperatively, this needs to be automated for clinical feasibility.
4. The α value is constant for all spring points, but could be adaptive depending on where the spring points are between the vertebrae.
5. The registration pipeline is extensive so it would be useful if steps were only included if the registration accuracy was not clinically acceptable with a simpler version of the pipeline.
6. The registration pipeline needs to be executed on a larger number of patient datasets to determine if the registration is reliable. This is currently in progress.
7. The registration pipeline should be validated on patient data where a gold standard is available. This will confirm the results attained in this thesis as a gold standard was not available.

Bibliography

- [1] M. Balki, Y. Lee, S. Halpern, and J. Carvalho. Ultrasound imaging of the lumbar spine in the transverse plane: the correlation between estimated and actual depth to the epidural space in obese parturients. *Anesthesia & Analgesia*, 108(6):1876–1881, 2009.
- [2] A. Belaid, D. Boukerroui, Y. Maingourd, and J.-F. Lerallut. Phase-based level set segmentation of ultrasound images. *IEEE Transactions on Information Technology in Biomedicine*, 15(1):138–147, 2011.
- [3] P.J. Besl and N.D. McKay. Method for registration of 3-D shapes. *IEEE Transactions on Pattern Analysis and Machine Intelligence*, 14(2):239–256, 1992.
- [4] W.E. Brant and C.A. Helms. *Fundamentals of diagnostic radiology*. Wolters Kluwer Health, Philadelphia, PA, USA, 2012.
- [5] C.R. Broadbent, W.B. Maxwell, R. Ferrie, D.J. Wilson, M. G.-C., and R. Russell. Ability of anaesthetists to identify a marked lumbar interspace. *Anaesthesia*, 55(11):1122–1126, 2000.

- [6] A. Brounstein, I. Hacihamoglu, P. Guy, A. Hodgson, and R. Abugharbieh. Towards real-time 3D US to CT bone image registration using phase and curvature feature based GMM matching. in *proc. of Medical Image Computing and Computer-Assisted Intervention (MICCAI)*, 235–242, Toronto, ON, Canada, 2011.Mi
- [7] P. Čech, A. Andronache, L. Wang, G. Székely, and P. Cattin. Piecewise rigid multimodal spine registration. in *proc. of Bildverarbeitung für die Medizin*, 211–215., Hamburg, Germany, 2006.
- [8] C.S. Chan, D.C Barratt, P.J. Edwards, G.P. Penney, M. Slomczykowski, T.J. Carter, and D.J. Hawkes. Cadaver validation of the use of ultrasound for 3D model instantiation of bony anatomy in image guided orthopaedic surgery. in *proc. of Medical Image Computing and Computer-Assisted Intervention (MICCAI)*, 397–404, Saint-Malo, France, 2004.
- [9] K. J. Chin, R. Ramlogan, C. Arzola, M. Singh, and V. Chan. The utility of ultrasound imaging in predicting ease of performance of spinal anesthesia in an orthopedic patient population. *Regional Anesthesia and Pain Medicine*, 38(1):34–38, 2013.
- [10] H. Chui and A. Rangarajan. A new point matching algorithm for non-rigid registration. *Computer Vision and Image Understanding*, 89(2):114–141, 2003.
- [11] K. Cleary, M. Clifford, D. Stoianovici, M. Freedman, S.K. Mun, and V. Watson. Technology improvements for image-guided and minimally invasive spine procedures. *IEEE Transactions on Information Technology in Biomedicine*, 6(4):249–261, 2002.

- [12] P.H. Conroy, C. Luyet, C.J. McCartney, and P.G. McHardy. Real-time ultrasound-guided spinal anaesthesia: a prospective observational study of a new approach. *Anesthesiology Research & Practice*, 2013:525818–525824, 2013.
- [13] Ascension Technology Corporation. 3D guidance trakstar. http://www.ascension-tech.com/medical/pdf/trakSTAR_SpecSheet.pdf, 2012. Accessed: 2013-06-10.
- [14] W.R. Crum, T. Hartkens, and D.L.G. Hill. Non-rigid image registration: theory and practice. *British Journal of Radiology*, 77(2):S140–S153, 2004.
- [15] F.J.E. Falco, L. Manchikanti, S. Datta, N. Sehgal, S. Geffert, O. Onyewu, J. Zhu, S. Coubarous, M. Hameed, S.P. Ward, M. Sharma, H. Hameed, V. Singh, and M.V. Boswell. An update of the effectiveness of therapeutic lumbar facet joint interventions. *Pain Physician*, 15:E909–E953, 2012.
- [16] A. Fedorov, K. Tuncali, F.M. Fennessy, J. Tokuda, N. Hata, W.M. Wells, R. Kikinis, and C.M. Tempany. Image registration for targeted MRI-guided transperineal prostate biopsy. *Journal of Magnetic Resonance Imaging*, 36(4):987–992, 2012.
- [17] P. Foroughi, E. Boctor, M.J. Swartz, R.H. Taylor, and G. Fichtinger. Ultrasound bone segmentation using dynamic programming. in *proc. of IEEE Ultrasonics Symposium*, 2523–2526, New York, NY, USA, 2007.
- [18] K. Galiano, A. A. Obwegeser, C. Walch, R. Schatzer, F. Ploner, and H. Gruber. Ultrasound-guided versus computed tomography-controlled facet joint injections

- in the lumbar spine: a prospective randomized clinical trial. *Regional Anesthesia and Pain Medicine*, 32(4):317–322, 2007.
- [19] S. Gill, P. Abolmaesumi, G. Fichtinger, J. Boisvert, D. Pichora, D. Borshneck, and P. Mousavi. Biomechanically constrained groupwise ultrasound to CT registration of the lumbar spine. *Medical Image Analysis*, 16(3):662–674, Apr 2012.
 - [20] I. Hacihaliloglu, R. Abugharbieh, A.J. Hodgson, and R.N. Rohling. Bone surface localization in ultrasound using image phase-based features. *Ultrasound in Medicine & Biology*, 35(9):1475–1487, 2009.
 - [21] I. Hacihaliloglu, R. Abugharbieh, A.J. Hodgson, R.N. Rohling, and P. Guy. Automatic bone localization and fracture detection from volumetric ultrasound images using 3-d local phase features. *Ultrasound in Medicine & Biology*, 38(1):128–144, 2012.
 - [22] I. Hacihaliloglu, A. Rasoulian, R. Rohling, and P. Abolmaesumi. Statistical shape model to 3d ultrasound registration for spine interventions using enhanced local phase features. accepted in *proc. of Medical Image Computing and Computer-Assisted Intervention (MICCAI)*, Nagoya, Japan, 2013.
 - [23] T. Heimann and H.-P. Meinzer. Statistical shape models for 3D medical image segmentation: A review. *Medical Image Analysis*, 13(4):543–563, 2009.
 - [24] J.B. Hummel, M.R. Bax, M.L. Figl, Y. Kang, C. Maurer, W. W Birkfellner, H. Bergmann, and R. Shahidi. Design and application of an assessment protocol for electromagnetic tracking systems. *Medical Physics*, 32(7):2371–2379, 2005.

- [25] L. Ibanez, W. Schroeder, L. Ng, and J. Cates. *The ITK software guide: The Insight Segmentation and Registration Toolkit (Version 2.4)*. Kitware Inc., Clifton Park, NY, USA, 2003.
- [26] A.K. Jain and R.H Taylor. Understanding bone responses in B-mode ultrasound images and automatic bone surface extraction using a bayesian probabilistic framework. *in proc. of SPIE medical imaging*, 5373:131–142, San Diego, CA, USA, 2004.
- [27] B.A. Johnson, K.P. Schellhas, and S.R. Pollei. Epidurography and therapeutic epidural injections: technical considerations and experience with 5334 cases. *American Journal of Neuroradiology*, 20(4):697–705, 1999.
- [28] H.J. Johnson, G. Harris, and K. Williams. Brainsfit: Mutual information registrations of whole-brain 3D images, using the insight toolkit. *The Insight Journal*, 2007.
- [29] D.J. Kopacz, J.M. Neal, and J.E. Pollock. The regional anesthesia “learning curve”: What is the minimum number of epidural and spinal blocks to reach consistency? *Regional Anesthesia and Pain Medicine*, 21(3):182–190, 1996.
- [30] P. Kovesi. *Invariant measures of image features from phase information*. PhD thesis, University of Western Australia, Crawley, WA, Australia, 1996.
- [31] O. Kutter, R. Shams, and N. Navab. Visualization and GPU-accelerated simulation of medical ultrasound from CT images. *Computer Methods and Programs in Biomedicine*, 94(3):250–266, 2009.

- [32] A. Lasso, T. Heffter, C. Pinter, T. Ungi, and G. Fichtinger. Implementation of the PLUS open-source toolkit for translational research of ultrasound-guided intervention systems. in *proc. of Medical Image Computing and Computer-Assisted Intervention (MICCAI), Workshop on Systems and Architectures for Computer Assisted Interventions*, 1–12, Nice, France, 2012.
- [33] S.S. Liu, J.E. Ngeow, and J.T. YaDeau. Ultrasound-guided regional anesthesia and analgesia: a qualitative systematic review. *Regional Anesthesia and Pain Medicine*, 34(1):47–59, 2009.
- [34] S.S. Liu, W.M. Strodtbeck, J.M. Richman, and C.L. Wu. A comparison of regional versus general anesthesia for ambulatory anesthesia: a meta-analysis of randomized controlled trials. *Anesthesia & Analgesia*, 101(6):1634–1642, 2005.
- [35] T. Liu, D. Shen, and C. Davatzikos. Deformable registration of cortical structures via hybrid volumetric and surface warping. *NeuroImage*, 22(4):1790–1801, 2004.
- [36] B. Ma and R.E. Ellis. Robust registration for computer-integrated orthopedic surgery: laboratory validation and clinical experience. *Medical Image Analysis*, 7(3):237–250, 2003.
- [37] J.M. Mathis and S. Golovac. *Image Guided Spine Interventions*. Springer, New York, NY, USA, 2010.
- [38] M.H. Moghari and P. Abolmaesumi. Point-based rigid-body registration using an unscented Kalman filter. *IEEE Transactions on Medical Imaging*, 26(12):1708–1728, 2007.

- [39] M. Mulet-Parada and J.A. Noble. 2D+T acoustic boundary detection in echocardiography. *Medical Image Analysis*, 4(1):21–30, 2000.
- [40] A. Myronenko and X. Song. Point set registration: coherent point drift. *IEEE Transactions on Pattern Analysis and Machine Intelligence*, 32(12):2262–2275, 2010.
- [41] S. Narouze and P.W.H. Peng. Ultrasound-guided interventional procedures in pain medicine: a review of anatomy, sonoanatomy, and procedures: part ii: axial structures. *Regional Anesthesia and Pain Medicine*, 35(4):386–396, 2010.
- [42] J.A. Noble and D. Boukerroui. Ultrasound image segmentation: a survey. *IEEE Transactions on Medical Imaging*, 25(8):987–1010, 2006.
- [43] P.W.H. Peng and S. Narouze. Ultrasound-guided interventional procedures in pain medicine: a review of anatomy, sonoanatomy, and procedures: part i: non-axial structures. *Regional Anesthesia and Pain Medicine*, 34(5):458–474, 2009.
- [44] G.P. Penney, D.C. Barratt, C.S. Chan, M. Slomczykowski, T.J. Carter, P.J. Edwards and D.J. Hawkes. Cadaver validation of intensity-based ultrasound to CT registration. *Medical Image Analysis*, 10(3):385–395, 2006.
- [45] T.M. Peters and K.R. Cleary. *Image-guided Interventions: Technology and Applications*. Springer, New York, NY, USA, 2008.
- [46] S. Pieper, M. Halle, and R. Kikinis. 3D slicer. in *proc. of IEEE International Symposium on Biomedical Imaging: Nano to Macro*, 632–635, Arlington, VA, USA, 2004.

- [47] S. Pieper, B. Lorensen, W. Schroeder, and R. Kikinis. The NA-MIC kit: ITK, VTK, pipelines, grids and 3D slicer as an open platform for the medical image computing community. in *proc. of IEEE International Symposium on Biomedical Imaging: Nano to Macro*, 698–701. Arlington, VA, USA, 2006.
- [48] V. Racic, A. Pavic, and J.M.W. Brownjohn. Experimental identification and analytical modelling of human walking forces: Literature review. *Journal of Sound and Vibration*, 326(12):1 – 49, 2009.
- [49] K. Rajpoot, V. Grau, and J.A. Noble. Local-phase based 3D boundary detection using monogenic signal and its application to real-time 3-D echocardiography images. in *proc. of IEEE International Symposium on Biomedical Imaging: From Nano to Macro*, 783–786, Boston, MA, USA, 2009.
- [50] A. Rasoulian, R. Rohling, and P. Abolmaesumi. Probabilistic registration of an unbiased statistical shape model to ultrasound images of the spine. in *proc. of SPIE Medical Imaging*, 8316:83161P-1–83161P-6, Orlando, Florida, USA, 2012.
- [51] A. Rasoulian, P. Abolmaesumi, and P. Mousavi. Feature-based multibody rigid registration of CT and ultrasound images of lumbar spine. *Medical Physics*, 39(6):3154–3166, 2012.
- [52] A. Rasoulian, R. Rohling, and P. Abolmaesumi. Lumbar spine segmentation using a statistical multi-vertebrae anatomical shape+pose model. Available online in *IEEE Transactions on Medical Imaging*, Jun 2013.

- [53] D.B. Russakoff, T. Rohlfing, J.R. Adler Jr, and C.R. Maurer Jr. Intensity-based 2D-3D spine image registration incorporating a single fiducial marker. *Academic Radiology*, 12(1):37–50, 2005.
- [54] R. Shams, R. Hartley, and N. Navab. Real-time simulation of medical ultrasound from CT images. in *proc. of Medical Image Computing and Computer-Assisted Intervention (MICCAI)*, 734–741, New York, NY, USA, 2008.
- [55] R. Silbergbeit, B.A. Mehta, W.P. Sanders, and S.J. Talati. Imaging-guided injection techniques with fluoroscopy and CT for spinal pain management1. *Radiographics*, 21(4):927–939, 2001.
- [56] T. Ungi, P. Abolmaesumi, R. Jalal, M. Welch, I. Ayukawa, S. Nagpal, A. Lasso, M. Jaeger, D. Borschneck, G. Fichtinger, et al. Spinal needle navigation by tracked ultrasound snapshots. *IEEE Transactions on Biomedical Engineering*, 59(10):2766–2772, 2012.
- [57] W. Wein, S. Brunke, A. Khamene, M.R. Callstrom, and N. Navab. Automatic CT-ultrasound registration for diagnostic imaging and image-guided intervention. *Medical Image Analysis*, 12(5):577–585, 2008.
- [58] W.M. Wells III. Statistical approaches to feature-based object recognition. *International Journal of Computer Vision*, 21(1-2):63–98, 1997.
- [59] A. H. White, R. Derby, and G. Wynne. Epidural injections for the diagnosis and treatment of low-back pain. *Spine*, 5(1):78–86, 1980.

- [60] R.E. Windsor, S. Storm, and R. Sugar. Prevention and management of complications resulting from common spinal injections. *Pain Physician*, 6(4):473–484, 2003.
- [61] S. Winter, B. Brendel, I. Pechlivanis, K. Schmieder, and C. Igel. Registration of CT and intraoperative 3-D ultrasound images of the spine using evolutionary and gradient-based methods. *IEEE Transactions on Evolutionary Computation*, 12(3):284–296, 2008.
- [62] B.J. Wood, H. Zhang, A. Durrani, N. Glossop, S. Ranjan, D. Lindisch, E. Levy, F. Banovac, J. Borgert, S. Krueger, J. Kruecker, A. Viswanathan, and K. Cleary. Navigation with electromagnetic tracking for interventional radiology procedures: a feasibility study. *Journal of Vascular and Interventional Radiology*, 16(4):493–505, 2005.
- [63] C.X.B. Yan, B. Goulet, J. Pelletier, S. J.-S. Chen, D. Tampieri, and L.D. Collins. Towards accurate, robust and practical ultrasound-CT registration of vertebrae for image-guided spine surgery. *International Journal of Computer Assisted Radiology and Surgery*, 6(4):523–537, Jul 2011.
- [64] C.X.B. Yan, B. Goulet, D. Tampieri, and L.D. Collins. Ultrasound-CT registration of vertebrae without reconstruction. *International Journal of Computer Assisted Radiology and Surgery*, 7(6):901–909, Nov 2012.
- [65] Z. Zhang. Iterative point matching for registration of free-form curves and surfaces. *International Journal of Computer Vision*, 13(2):119–152, 1994.